STUDIES ON THE PHYSICAL PROPERTIES OF WOOD IN RELATION TO THE FINE STRUCTURES OF CELL WALL

（木材の各種物性と細胞壁微細構造との関連性についての研究）

2004

YOICHI KOJIMA

STUDIES ON THE PHYSICAL PROPERTIES OF WOOD IN RELATION TO THE FINE STRUCTURES OF CELL WALL

(木材の各種物性と細胞壁微細構造との関連性についての研究)

by

Yoichi KOJIMA

Laboratory of Biomaterial Physics

Division of Biological Material Sciences

Department of Biosphere Resources Science

The Graduate School of Bioagricultural Science

Nagoya University

Nagoya, 464, JAPAN

報告番号	甲第 6157 号

CONTENTS

GENERAL INTRODUCTION

In wood cell wall, highly crystallized cellulose microfibril (CMF) is formed during the xylem cell maturation. The CMF in each lamella is oriented in a certain direction to the fiber axis, therefore, the structure and physical property of the CMF highly affect to the physical properties of wood. The orientation of the CMF is different among each cell wall lamella. Moreover, the CMF was surrounded by the matrix substance of lignin-hemicellulose, therefore, the origin of the physical properties of wood is more or less affected by the properties of the matrix substance in spite that the Young's modulus of the cellulose crystal is much larger than the matrix substance.

For example, the physical properties of wood are highly affected by the temperature and the moisture. The origin of such phenomena should be clarified from the viewpoint of the macro-molecule level of the constituents of the cell wall, namely, CMF and matrix substance.

Many studies have been conducted on the relationship between the fine structure and physical property of wood. However, most of those conclusions are individualized ones, which are estimated from each phenomenon. Therefore, general theory which can explain many phenomena at the same time without any contradiction has not been given yet. This is the main reason that it is still difficult to understand the origins of various physical properties of wood on the basis of a general model of the fine structure of wood cell wall. Especially, role of the interfacial structure of the CMF and matrix substance is essentially unsolved. In this situation, no matter how the data and the observation are accomplished at the molecular level by using isolated constituent materials, those results should not be deduced to the theory to explain the properties of the cell wall or wood.

Some physical behaviors of the wood are described numerically based on "the reinforced-matrix hypothesis" originally proposed by Barber and Meylan (1964). This hypothesis is useful for formulating the mechanical interaction between the CMF bundle and the matrix skeleton on the basis of "two-phase structure". The physical properties and mechanical behaviors of wood can be simulated by using the structural model of wood fiber which is constructed by the reinforced-matrix hypothesis.

Besides, the mechanical model derived on the basis of the reinforced-matrix hypothesis contains various parameters which characterize the composite structure of each layer and the physical property of each constituent material. It is considered that information on the fine structures and the internal properties of each cell wall constituent are dispersed and incorporated into those parameters. When comparing the simulated results with the experimental one, the author needs to give concrete values to those parameters in a rational manner. Then it is quite natural to consider that the values of the parameters given in the simulation reflect intrinsic information on the fine structure and the internal properties of the cell wall constituents.

In this thesis, based on the above background, the author tried to explain the relationships between the some physical properties of wood and the fine structure of the cell wall. Among the physical properties of wood at the macroscopic level, it is very important to clarify the physical properties in the longitudinal direction since the longitudinal properties of wood reflects the properties of wood cell wall more directly. The author focused the longitudinal elastic property and viscoelastic property of clear wood specimen.

In Chapter 1, the author looked back on the history of the studies about the relationships between the physical properties of wood and the fine structure of the cell wall.

In Chapter 2, the author developed the mathematical model which predicts the longitudinal Young's modulus of a clear wood specimen on the basis of the reinforced-matrix hypothesis, and gave some case studies on the elastic behaviors of the wood by using the newly-developed model. Then, some possibilities (predictions) on the structures and the moisture properties of the CMF and the matrix substance were proposed.

In Chapter 3, propriety of the possibilities (predictions) proposed in Chapter 2 were discussed through both the experimentation using a sugi microtomed specimen and the simulation using the wood fiber model.

In above Chapters, the author thought that wood is an elastic body, however, it is also important to clarify the viscoelastic properties of wood cell wall in order to use forest products as structural member for buildings or furniture. There are few reports on

the longitudinal tensile tests in relation to the viscoelastic properties of wood. Moreover, the relationship between the viscoelastic properties and the fine structure of wood cell wall has not been solved yet. Then, in Chapter 4, the author tried to clarify the longitudinal tensile creep behavior in relation to the fine structure of wood cell wall.

Finally, the author induced the results obtained in the above Chapters as general conclusion.

CHAPTER 1 BACKGROUND

1.1 Modelling of the physical properties of wood

For better understanding of the origins of the mechanical and physical properties of wood, it is required to reveal the fine structures and microscopic properties of each cell wall constituent as it is in the cell wall. Moreover, it is indispensable to obtain a proper theory which deduces the microscopic information on the cell wall constituents into the macroscopic behaviors of the wood.

With the progress of a technique for the microscopic observation through the 1950s into 1960s, it was revealed that each cell wall lamella can be approximated as a "two-phase structure" consisting of the cellulose microfibril (CMF) as a framework bundle and the lignin-hemicellulose as a matrix skeleton.

"The reinforced-matrix hypothesis" was proposed by Barber and Meylan (1964). Their idea was useful for formulating the mechanical interaction between the CMF bundle and the matrix skeleton on the basis of "the two-phase structure". Thereafter, several researchers adopted Barber and Meylan's idea and applied it to their own theoretical model. At present, this idea seems to be feasible to describe some physical behaviors of the wood numerically, including 1) shrinkage and swelling properties, 2) longitudinal Young's modulus, and 3) growth stress generation.

As the researches of the swelling and shrinking properties, a theoretical model that each wood cell wall was treated as a thick-wall circular cylinder was proposed by Barber (1968). In his model, all microfibrils lay at the same angle θ to the longitudinal axis so that they wind helically around the cell. Then, Barber and Meylan's theory was reformulated using a fundamental shrinkage relation derived for fiber-reinforced composite materials (Cave 1972a, 1972b). The theory was extended to include consideration of the variation (due to changes in moisture content) of the stiffness of the matrix that binds the cellulose microfibrils together. With the theory developed, it was possible to specify shrinkage with respect to moisture content, as well as with factors involved in cell-wall geometry and composition. Shrinkage behavior of the cell wall layers was related to constituent behavior through the use of "mechanics of materials" techniques and "energy methods" (Barrett et al. 1972). Double cell wall behavior was

determined by regarding the cell wall as a multi-layered structure composed of orthotropic layers oriented at angles to the cell-axis direction. Double cell wall model were used to assess effects of microfibril angle, layer thickness, and chemical composition of the wall on the shrinkage behavior of a typical early-wood, late-wood, and compression wood cell (Cave 1972a, 1972b, Barrett et al. 1972). A model was developed for estimating shrinkage property of a soft wood cell wall from the properties of its polymeric constituents: cellulose, hemicellulose and lignin (Koponen et al. 1989). The model took into account the helical winding of the microfibrils in the cell wall and it estimated the behavior of a balanced laminated double-cell wall in which rotation was restrained by adjacent cells. Yamamoto et al. (1999, 2001) simulated the shrinking process of a single wood fiber regarding water desorption to elucidate the origin of the shrinking anisotropy of wood during the drying process, as well as to begin to gain an understanding of the interaction between the moisture and the cell wall components. The wood fiber model used for the simulation was a complex circular cylinder having three layers. It consisted of the compound middle lamella (CML), the outermost and the middle layers of the secondary wall (S1 and S2, respectively). The microfibril angles (MFA) took 90 degrees in the S1 layer and a value between 0-60 degrees in the S2 layer.

As the researches of the origin of the longitudinal Young's modulus, Cave (1978a, 1978b) constructed a double-walled model that simultaneously predicted the variation with the moisture content change of the longitudinal Young's modulus of wood. Koponen et al. (1989) developed a model for estimating elastic property of a softwood cell wall from the properties of its polymeric constituents: cellulose, hemicellulose and lignin. In this model, the cell wall consisted of layers M+P, S1, S2 and S3, and two adjacent cell walls were examined as a unit. The secondary wall consisted of microfibrils embedded in lignin and the middle lamella consisted of lignin only. Thereafter, Yamamoto and Kojima (2002) developed the theory by using a multi-layered circular cylinder model, which can simulate the elastic behaviors of the clear wood specimen more realistically in relation to the change of moisture content.

As the research of the growth stress, Yamamoto (1998, in press) tried to explain the generation mechanism of tree growth stresses in relation to time and location inhomogeneity in the secondary wall lignification, and he made a theoretical discussion

on the generation process of the growth strain (maturation strain) by using a complex circular cylinder, CML+S1+S2, or CML+S1+S2+G (gelatinous layer).

1.2 Physical properties of cell wall constituents

In the simulation of the physical properties of wood by using theoretical model, the values of each parameter in the model should be determined in advance. Some of them have already been known by experiments and observations. For instance, the axial Young's modulus of pure cellulose crystal, that of amorphous cellulose in the framework bundle, and that of isotropic matrix substance are important parameters in addition to their proportions in each cell wall layer. From the macroscopic observations, thickness of the each cell wall lamella and the value of the MFA are easily revealed.

The value of the axial Young's modulus of the cellulose crystal was measured using bleached ramie (Sakurada et al. 1962, 1964). The lattice extension was measured by x-ray diffraction under a constant stress. The obtained elastic modulus was 137×10^4kgf/cm^2 (=134GPa). Moreover, Nishino et al. (1995) measured the crystal modulus in the direction parallel to the chain axis of five kinds of cellulose polymorphs by x-ray diffraction. They also suggested that the crystal modulus of cellulose I was 138GPa. On the other hand, Ishikawa et al. (1997,1998) tried to estimate the Young's modulus of the amorphous cellulose by using ramie fiber. They determined it 4-8GPa in the air-dried condition.

The axial Young's modulus of the isotropic matrix substance was determined by isolating it (Srinivasan 1941, Cousins 1976, 1978). They revealed that the Young's modulus of the molded matrix substance takes a value of 20×10^3kgf/cm^2 (=1.96GPa) above the fiber saturation point, then, it increases monotonously depending on the water desorption, and it reaches values of 4-6GPa at the oven-dried state.

1.3 Longitudinal elastic properties of wood

The longitudinal young's modulus of wood is highly affected by the MFA in the S2 layer. The relationship between the longitudinal Young's modulus and MFA was measured using *Pinus radiata* (Cave 1968). Sobue and Asano (1976) also measured the Longitudinal Young's modulus in relation to the MFA using a sugi thin specimen.

Moreover, Page et al. (1977) tried to measure the longitudinal Young's modulus using an isolated softwood (black spruce) fiber. Page's data was based on the fibers prepared from a holocellulose pulp and a kraft pulp of 45% yield. Above three experimental results conformed that the longitudinal Young's modulus tends to decrease as the MFA in the S2 layer increases.

Furthermore, origin of the MFA dependency of the longitudinal Young's modulus was explained on the basis of the theoretical models having unidirectionally reinforced cell walls. Cave (1968, 1972b, 1978b), and Sobue and Asano (1976) simulated the relationship between the longitudinal Young's modulus and MFA by using the double cell wall model. Salmen (1982), Salmen and De Ruvo (1985) and Salmen et al. (1985) confirmed the importance of the MFA in the S2 layer by using the model which was based on assuming each cell wall layer to consist of cellulose microfibrils embedded in a matrix of hemicellulose. The lignin was considered to exist in separate isotropic lamellae located in the middle of each cell wall layer. Koponen (1991) developed a model based on wood structure for estimating the elastic properties of softwoods. The wood model consisted of early-wood, late-wood and ray cells, each of which has a different cell wall structure. The calculated elastic properties were good agreement with test results.

The Longitudinal Young's modulus is also highly affected by the moisture content. The longitudinal Young's modulus of wood decreases as the moisture content increases up to FSP, and becomes constant above FSP (Kollmann and Krech 1960). Furthermore, the longitudinal Young's modulus of wood tends to decrease to 60-70% of the initial value from the oven-dried state to FSP (e.g. Kollmann and Krech 1960).

It is generally believed that the reduction of the Young's modulus of wood due to the increase of the moisture content is caused mainly by the hygrosoftening of the matrix substance which is an isotropic mixture of lignin, hemicellulose, and amorphous domain of the CMF bundle (e.g. Norimoto and Yamada 1967). If this suggestion would be true, the reduction of the longitudinal Young's modulus due to water desorption should be more remarkable in specimen with large MFA than with small MFA, which was pointed out theoretically by Salmen (1982). However, this suggestion was contradicted by the experimental result (Kojima and Yamamoto in press).

1.4 Viscoelastic properties of wood

It is very important to clarify the viscoelastic properties of wood cell wall in order to use forest products as structural member for buildings or furniture. Studies on the viscoelastic properties of wood began on a large scale in the 1960s (e.g. Yamada et al 1961), and included creep and stress relaxation.

It is well known that the viscoelastic properties of wood are highly affected by many factors, for example; moisture, temperature, and fine structure of cell wall etc. In this section, the reports about the viscoelastic properties of wood were shortly given.

As the researches of the relationship between the viscoelastic properties and the temperature, Kitahara and Yukawa (1964) studied the extent of the influence of change of temperature on creep in the midst creep. Moreover, the influence of high temperature (100~180℃) on the creep of Hinoki (*Chamaecyparis obtusa* ENDL.) was investigated by compressive test in oven-dried condition (Arima 1967).

As the researches of the relationship between the viscoelastic properties and the moisture content, studies on the mechano-sorptive creep behavior were begun (Armstrong 1972, Armstrong and Kingston 1960, Armstrong and Christensen 1961). They reported that creep in wooden beam markedly increased when its moisture content changed while it was under load. The deflection of a loaded beam that is taken through one or more cycles of humidity increases far beyond the deflection of beams loaded after they have been conditioned to either of the extreme moisture contents. After extensive moisture cycling, such a deflection increases during the drying part of the cycles and decreases during wetting. Then, Grossman (1976) reviewed characteristic features of the effect of simultaneous moisture change and load on the deformation of wood.

As the researches of the relationship between the viscoelastic properties and the fine structure of cell wall, the stress relaxation of delignified wood (Hinoki) which are obtained by the stepwise treatments with acidified sodium chlorite solution was measured (Fushitani 1968a~d). The stress relaxation was studied by three points bending test in both air-dried and water-saturated condition. According to his results, residual lignin content has a big effect on the stress relaxation. The studies on the rheological behaviors of wood during decrystallization were conducted (Aoki and

Yamada 1977). It has been reported that wood is decrystallized markedly with the mixture of diethyl amine, sulfur dioxide and dimethyl sulfoxide (DMSO) and decrystallized wood is easily recrystallized by immersing in water. In this study, the temperature dependence of torsional creep of wood during decrystallization and of the decrystallized wood were examined. As a result, Creep compliance increased in proportion to degree of decrystallization. Moreover, the relations between crystal lattice strain of (004) plane and surface strain at different moisture content, and behavior of during creep and stress relaxation were examined (Moriizumi and Okano 1978). As a result, crystal lattice strain changes with time; it increases during creep, while it decreases during stress relaxation.

As the research of the relationship between the viscoelastic properties and acoustic emission, the relationships between the bending creep behaviors and the acoustic emission (AE) characteristics of wood under changing moisture conditions were measured (Ozawa et al. 1995). It was found that creep strain was not related closely to the cumulative AE event counts for all of the moisture conditions.

There are no reports which apply the reinforced-matrix hypothesis to the viscoelastic properties. Moreover, the behavior of wood cell wall constituent materials to the viscoelastic properties of wood has not been revealed yet.

CHAPTER 2 FORMULATION OF THE LONGITUDINAL ELASTICITY OF AN ISOLATED WOOD FIBER

2.1 Introduction

For better understanding of the origins of the mechanical and physical properties of wood, it is required to reveal the fine structure and microscopic properties of each cell wall constituent. Moreover, it is indispensable to obtain a proper theory which deduces the microscopic information on the cell wall constituents into the macroscopic behaviors of the wood. With the progress of a technique for the microscopic observation through the 1950s into the 1960s, it was revealed that each cell wall lamella can be approximated as a "two-phase structure" consisting of the cellulose microfibril (CMF) as a framework bundle and the lignin-hemicellulose as a matrix skeleton.

"The reinforced-matrix hypothesis" was proposed by Barber and Meylan (1964). Their idea was useful for formulating the mechanical interaction between the CMF bundle and the matrix skeleton on the basis of "the two-phase structure". Thereafter, several researchers adopted Barber and Meylan's idea and applied it to their own theoretical models. At present, this idea seems to be feasible to describe some physical behaviors of the wood numerically, for example, the growth stress generation (Yamamoto 1998), the swelling anisotropy (Barber 1968, Cave 1972a, 1972b, Barrett et al. 1972, Koponen et al. 1989, Yamamoto et al. 2001), and the origin of the longitudinal Young's modulus (Cave 1978a, 1978b, Koponen et al. 1991). However, the idea of "the two-phase structure" is effective only at the level larger than the cell wall layer, therefore, it is improper to apply the reinforced-matrix hypothesis for elucidating the internal properties and fine structures of each cell wall constituent directly as it is in the cell wall lamella.

Besides, the mechanical model derived on the basis of the reinforced-matrix hypothesis contains various parameters derived from "two-phase approximation". It is considered that information on the fine structures and the internal properties of each cell wall constituent are dispersed and incorporated into those parameters. When comparing the simulated results with the experimental one, the author needs to give concrete values to those parameters in a rational manner. Then it is quite natural to consider that the

values of the parameters optimized in the simulation reflect intrinsic information on the fine structure and internal properties of the cell wall constituents.

In the previous study, adopting Barber's (1968) circular cylinder model consisting of the S2 layer, which is a developed version of Barber and Meylan's original one, Yamamoto (1999) and Yamamoto et al. (2001) generalized it into the one having a multi-layered cell wall. Moreover, they formulated the dynamics of the anisotropic shrinkage of the wood fiber during the moisture adsorption by using the newly generalized model.

In this chapter, the author tries to develop it into the one which predicts the longitudinal Young's modulus of the wood in relation to the moisture content. Then, it is anticipated to estimate the fine structure and internal properties of the cell wall constituents peculiar to the wood by examining the values of the parameters which are optimized through the simulation.

2.2 Modelling the origin of the longitudinal Young's modulus and the Poisson's ratio by the reinforced matrix hypothesis

2.2.1 Nomenclatures

E: Young's modulus of the CMF bundle in the direction parallel to the molecular chains of the cellulose. (Specifically to say, the value of E should be distinguished in respective layers. This is subdivided into E_u and E_S in the S1 and the S2 layer, respectively.)

S: Shear moduli (×2) of the matrix skeletons in each layer. S is denoted as S_I, S_u and S_S in the CML (compound middle lamella), the S1 and the S2 layers, respectively

M: $=S_S/S_u$

r_{in}: the inner radius of each layer. r_{in} is denoted as u_2, u_1 and r_1 in the CML, the S1 and the S2 layers, respectively

r_{out}: the outer radius of each layer. r_{out} is denoted as u_2+h, u_2 and r_2 ($=u_1$) in the CML, the S1 and the S2 layers, respectively

h: thickness of the CML layer

r, k, u: $r=r_{out}/r_{in}$. $k=r_2/r_1$. $u=u_2/u_1$.

θ: the microfibril angle (MFA)

P_{in}: boundary pressure acting on the inner surface of each layer. P_{in} is denoted as P_3, P_2 and 0 in the CML, the S1 and the S2 layers, respectively

P_{out}: boundary pressure acting on the outer surface of each layer. P_{out} is denoted as 0, P_3 and P_2 in the CML, the S1 and the S2 layers, respectively

$\hat{L}_0$, $\tilde{L}_0$, L_0: the tensile or compressive loads induced in the CML, the S1 and the S2 layers, respectively

G: $=E/S$. G is denoted as G_I, G_u and G_S in the CML, the S1 and the S2 layers, respectively

ε_L, ε_T ,ε_R: respectively, the longitudinal, the tangential and the radial normal strains induced at every point of the wood fiber model

ε_T^{u2}: $= [\varepsilon_T(r)]_{r=u2}$. tangential normal strain induced at the outer surface of the S1 layer ($r=u_2$)

ε_T^{u1}: $= [\varepsilon_T(r)]_{r=u1}$. tangential normal strain induced at the inner surface of the S1 layer ($r=u_1$)

α, ϕ, φ, $\tilde{e}$, $\tilde{q}$, $\tilde{r}$, e, q, q^*, a, b, p, B, H: See APPENDIX 1 and Table2-1.

2.2.2 Generalization of Barber's wood fiber model

In the previous study (Yamamoto et al. 1995), Barber's (1968) wood fiber model consisting of the compound middle lamella (CML) and the S2 layer was developed into a new one having the S1 layer between the CML and the S2 layer (Fig2-1). Moreover, formulated was the anisotropic shrinking process of the wood tracheid without any external force (Yamamoto 1999). In that model, each layer is composed of two parts, namely, the cellulose microfibril (CMF) bundle as the framework and the isotropic lignin-hemicellulose skeleton as the matrix. In the macroscopic limit, both the CMF bundle and the matrix skeleton can be considered to occupy the same domain. It is supposed that the CMFs in the S2 layer and the S1 layer are oriented in certain directions. On the other hand, the orientation of the CMF is randomly distributed in the CML, which can then be considered mechanically isotropic.

2.2.3 Formulation of the reinforced-matrix hypothesis by using the generalized Barber's wood fiber model

(a) Mechanical interaction between the matrix skeleton and the CMF bundle in the secondary wall

The deformation of the wood fiber model is assumed to be symmetric with respect to the central axis. Then a cylindrical coordinate system (O-LTR) can be applied to the present analysis. At every point in each layer of the secondary wall, a local orthogonal coordinate system, O-LTR, can be applied. The L, T and R-axes are in the longitudinal, tangential and radial directions, respectively, as shown in Fig.2-2.

A significant deformation induced at every point in each layer of the secondary wall is expressed by the observable strain tensor components ε_{ij} (i,j=L,T,R) in the O-LTR coordinate system. The deformation of the matrix skeleton is equal to that of the CMF bundle. Therefore, they are expressed by the same strain components.

The stress components induced in the matrix skeleton of each layer of the secondary wall σ_{ij}^{m} are related to the observable strain components ε_{ij} (i,j=L,T,R) as the following constitutive equation:

$$\sigma_{ij}^{m} = C_{ijkl}^{m}\varepsilon_{kl} \qquad \text{(Eq.2-1)}$$

The lignin-hemicellulose matrix as a skeleton is considered to be isotropic (Kerr and Goring 1975), then, elastic constants of the matrix skeleton (non zero terms) are denoted as

$$\begin{aligned} &C_{LLLL}^{m} = C_{TTTT}^{m} = C_{RRRR}^{m} = \lambda + 2\mu \\ &C_{LLTT}^{m} = C_{LLRR}^{m} = C_{TTLL}^{m} = C_{TTRR}^{m} = C_{RRLL}^{m} = C_{RRTT}^{m} = \lambda, \\ &C_{TRTR}^{m} = C_{RLRL}^{m} = C_{LTLT}^{m} = \mu \end{aligned} \qquad \text{(Eqs.2-2)}$$

with Lame's parameters

$$\lambda = \frac{\nu^{m}E^{m}}{(1-2\nu^{m})(1+\nu^{m})} \quad \text{and} \quad \mu = \frac{E^{m}}{2(1+\nu^{m})},$$

where E_m, ν_m are the Young's modulus and the Poisson's ratio of the matrix skeleton in each layer of the secondary wall, respectively.

By introducing new parameters

$K = 3\lambda + 2\mu, \quad S = 2\mu$,

the author can rewrite the elastic constants (Eqs.2-2) as follows,

$$\begin{aligned} &C_{LLLL}^{m} = C_{TTTT}^{m} = C_{RRRR}^{m} = \frac{1}{3}(K + 2S) \\ &C_{LLTT}^{m} = C_{LLRR}^{m} = C_{TTLL}^{m} = C_{TTRR}^{m} = C_{RRLL}^{m} = C_{RRTT}^{m} = \frac{1}{3}(K - S) \\ &C_{TRTR}^{m} = C_{RLRL}^{m} = C_{LTLT}^{m} = \frac{1}{2}S \end{aligned} \qquad \text{(Eqs.2-3)}$$

It is well recognized that the CMF bundle in each layer of the secondary wall consists of a transverse isotropic material whose principal axis (x-axis) is parallel to the direction of the molecular chains. Figure2-3 shows a small flat-board element of the CMF bundle in the S2 layer, provided that the positive direction of the normal axis (z-axis) is coincident with the radial direction (R-axis) of the fiber model. In this model, the CMF in the S2 layer is assumed to be oriented in a S-herix at an angle of θ.

The relationship between stress (σ_{ij}^{f*}) and strain (ε_{ij}^{*}) components induced in the CMF bundle of each layer of the secondary wall can be written as the following constitutive equation in the O-xyz orthogonal coordinate system,

$$\sigma_{ab}^{f*} = C_{abcd}^{f*} \cdot \varepsilon_{cd}^{*}, \qquad \text{(Eq.2-4)}$$

where C_{abcd}^{f*} is the elastic constant tensor of the CMF bundle in the S1 or the S2 layers

in the 0-xyz coordinate system whose non-zero terms are denoted as

$C^{f*}_{xxxx}, C^{f*}_{xxyy}, C^{f*}_{xxzz}(=C^{f*}_{xxyy}), C^{f*}_{yyyy}, C^{f*}_{yyzz}, C^{f*}_{zzzz}(=C^{f*}_{yyyy}), C^{f*}_{yzyz}, C^{f*}_{zxzx}, C^{f*}_{xyxy}(=C^{f*}_{yzyz})$.

The author supposed that the CMF bundle is considerably compliant in the transverse direction, therefore, all shear moduli, Poisson's ratios, and the Young's modulus in the transverse direction are small enough to be neglected. This means that the CMF cannot be kept in a bundle shape without a reinforcing agent. Then, the author may consider the stiffness components C^{f*}_{abcd} are all nil except $C^{f*}_{xxxx}(=E)$.

By transforming the coordinate system from 0-xyz into 0-LTR system, the non-zero terms of the stiffness components of the CMF bundle (C^{f}_{ijkl}) are expressed as

$$\begin{aligned} &C^{f}_{LLLL}=l^4E, C^{f}_{LLTT}=l^2m^2E, C^{f}_{LLLT}=-l^3mE, C^{f}_{TTLL}=l^2m^2E, C^{f}_{TTTT}=m^4E, \\ &C^{f}_{TTLT}=-lm^3E, C^{f}_{LTLL}=-l^3mE, C^{f}_{LTTT}=-lm^3E, C^{f}_{LTLT}=l^2m^2E, \end{aligned} \quad \text{(Eqs.2-5)}$$

where l=cosθ, m=sinθ, and E is the Young's modulus of the CMF bundle in the direction of the molecular chains. By using this formula, Eq.2-4 can be rewritten into a new expression based on the 0-LTR coordinate system as follows

$$\sigma^{f}_{ij}=C^{f}_{ijkl}\cdot\varepsilon_{kl}. \quad \text{(Eq.2-6)}$$

Then, the following non-zero stress components are obtained:

$$\begin{aligned} &\sigma^{f}_{L}=El^2(\varepsilon_L l^2+\varepsilon_T m^2), \sigma^{f}_{T}=Em^2(\varepsilon_L l^2+\varepsilon_T m^2), \\ &\tau^{f}_{LT}=-Elm(\varepsilon_L l^2+\varepsilon_T m^2), \end{aligned} \quad \text{(Eqs.2-7)}$$

provided that $\sigma^{f}_{L}=\sigma^{f}_{LL}, \sigma^{f}_{T}=\sigma^{f}_{TT}, \tau^{f}_{LT}=\sigma^{f}_{LT}, \varepsilon^{f}_{L}=\varepsilon^{f}_{LL}, \varepsilon^{f}_{T}=\varepsilon^{f}_{TT}$.Moreover, it is supposed that E_{LT}=0 when deriving Eqs.2-7, due to the assumption of the axisymmetrical deformation. Thus, the fact can be expressed that the torsional deformation of an individual fiber is completely restricted by the force of binding fibers inside the wood specimen.

According to the reinforced-matrix hypothesis, the CMF framework as a bundle and the lignin-hemicellulose matrix as a skeleton occupy the same domain in the macroscopic limit, therefore, the following conditions can be assumed as balance of the force in each layer of the secondary wall,

$$\sigma_{ij}=\sigma^{m}_{ij}+\sigma^{f}_{ij} \quad \text{(Eq.2-8)}$$

where σ_{ij} (i,j=L,T,R) are the stress components generated in the secondary wall. Then, by rearranging Eq.2-8 using Eqs.2-1, 2-3, 2-7 and the compatibility of the strains,

$$\varepsilon_R-\varepsilon_T=r\frac{d\varepsilon_T}{dr},$$

we obtain

$$\sigma_L = \left\{\frac{1}{3}(K+2S)+El^4\right\}\varepsilon_L + \left\{\frac{2}{3}(K-S)+El^2m^2\right\}\varepsilon_T + \frac{1}{3}(K-S)r\frac{d\varepsilon_T}{dr}$$
$$\sigma_T = \left\{\frac{1}{3}(K-S)+El^2m^2\right\}\varepsilon_L + \left\{\frac{1}{3}(2K+S)+Em^2\right\}\varepsilon_T + \frac{1}{3}(K-S)r\frac{d\varepsilon_T}{dr} \qquad \text{(Eqs.2-9)}$$
$$\sigma_R = \frac{1}{3}(K-S)\varepsilon_L + \frac{1}{3}(2K+S)\varepsilon_T + \frac{1}{3}(K+2S)r\frac{d\varepsilon_T}{dr}$$
$$\tau_{LT} = -Elm\left(\varepsilon_L l^2 + \varepsilon_T m^2\right), \quad \tau_{TR} = \tau_{RL} = 0$$

Among the shear stress components, only τ_{LT} is not null, which is an inevitable consequence from the assumption of the axisymmetrical deformation. τ_{LT} gives no effect upon the normal stress components, σ_L, σ_T and σ_R, therefore, it is not required to take the effect of τ_{LT} into consideration when calculating the dimentional change of the wood fiber model.

(b) Mechanical interaction between the matrix skeleton and the CMF bundle in the CML

In the compound middle lamella (CML), the author should consider E=0 in Eqs.2-5, 2-7 and 2-9. This does not mean that there is no CMF in the CML, but that mechanical contribution of the randomly distributed CMF framework in the CML should be isotropic.

(c) Dimensional change of each layer

Equations 2-9 are regarded as a simultaneous equation of ε_L, ε_T and $r d\varepsilon_T/dr$, and can be solved for ε_L. Then, we obtain

$$\left\{3S+2E\left(1-3m^2-3m^4\right)\right\}\varepsilon_L = \left(2+\frac{E}{S}m^4\right)\sigma_L - \left(1+\frac{E}{S}m^2l^2\right)\sigma_T - \left((1-\frac{E}{S}m^2\left(l^2-m^2\right)\right)\sigma_R$$

(Eq.2-10)

In deriving the Eq.2-10, it is assumed that the bulk modulus in the matrix skeleton (K) is sufficiently larger than E and S. This means, the Poisson's ratio of the matrix skeleton is almost 0.5 like a kind of elastomer.

To integrate the Eq.2-10 in the crosscut surface of the layer, the necessary

arrangements are as follows: solving the second and the third formulae in the Eqs.2-9 for ε_T and $r\mathrm{d}\varepsilon_T/\mathrm{d}r$, and eliminating the teram of σ_T by using the condition of the stress equilibrium (in the case of axisymmetry),

$$\sigma_T - \sigma_R = r\frac{\mathrm{d}\sigma_R}{\mathrm{d}r},$$

we obtain

$$\begin{aligned}\left(2S + Em^4\right)\varepsilon_T &= -\left(S + Em^2l^2\right)\varepsilon_L + r\frac{\mathrm{d}\sigma_R}{\mathrm{d}r},\\ \left(2S + Em^4\right)r\frac{\mathrm{d}\varepsilon_T}{\mathrm{d}r} &= Em^2\left(2 - 3m^2\right)\varepsilon_L - 2r\frac{\mathrm{d}\sigma_R}{\mathrm{d}r}.\end{aligned} \qquad \text{(Eqs.2-11)}$$

Moreover, eliminating the term of ε_T in the Eqs.2-11, a linear second order differential equation of r is obtained, namely,

$$r^2\frac{\mathrm{d}^2\sigma_R}{\mathrm{d}r^2} + 3r\frac{\mathrm{d}\sigma_R}{\mathrm{d}r} = Em^2\left(2 - 3m^2\right)\varepsilon_L \qquad \text{(Eq.2-12)}$$

Equation 2-12 can be solved under suitable boundary conditions:

in $r=r_{in}$ (inner surface of each layer), $\sigma_R = -P_{in}$, and

in $r=r_{out}$ (outer surface of each layer), $\sigma_R = -P_{out}$,

where P_{in} and P_{out} are the internal and external pressures, respectively, acting upon each layer. After solving Eq.2-12, σ_T can be derived from the condition of the stress equilibrium. Then, the author integrates Eq.2-10 over the crosscut area of the layer and assuming that ε_L is independent of r since the wood fiber model is an infinitely long circular cylinder. As athe result, the author obtains the following expression:

$$\alpha\cdot\varepsilon_L = \frac{2}{3}\cdot\frac{L_0}{S\left(r_{out}^2 - r_{in}^2\right)}\left(2 + Gm^4\right) + \frac{1}{S}\cdot\varphi\cdot P_{out} + \frac{1}{S}\cdot\varphi\cdot P_{in} \qquad \text{(Eq.2-13)}$$

provided that coefficients α, ϕ and φ are the functions of G ($=E/S$), θ and r ($=r_{out}/r_{in}$). L_0 is

$$L_0 = \frac{1}{2\pi}\int_{layer}\sigma_L\,\mathrm{d}A = \int_{r_{in}}^{r_{out}}\sigma_L r\,\mathrm{d}r.$$

In every layer of the secondary wall, it is required to give concrete values to the parameters, θ, r_{in}, r_{out}, r ($=r_{out}/r_{in}$), S, E, P_{in}, P_{out}, L_0, α, ϕ and φ in Eq.2-13, as shown in Table2-1.

(d) Dimensional change of the fiber as a whole

For each layer, Eq.2-13 can be rewritten as follows:

For the CML layer: as mentioned above, in this case, E should be 0, and S is denoted by S_I. Then, Eq.2-13 can be expressed as:

$$3F \cdot \hat{\varepsilon}_L = 2 \cdot \frac{\hat{L}_0}{u_2^2} - P_3, \qquad \text{(Eq.2-13')}$$

where $F=S_I h/u_2$, h is the thickness of the CML, and u_2 is the innermost radius of the CML.

For the S1 layer: in this case, E and S should be E_u and S_u, respectively. And θ is assumed to be 90 degrees. Then,

$$\tilde{e} \cdot \tilde{\varepsilon}_L = \frac{2}{3} \cdot \frac{\tilde{L}_0}{S_u\left(u_2^2 - u_1^2\right)}\left(2 + G_u\right) + \frac{1}{S_u} \cdot \tilde{q} \cdot P_2 + \frac{1}{S_u} \cdot \tilde{r} \cdot P_3, \qquad \text{(Eq.2-13")}$$

where u_2 and u_1 are the outermost and the innermost radii of the S1 layer, respectively.

For the S2 layer: in this case, E and S should be E_S and S_S, respectively. Then,

$$e \cdot \varepsilon_L = \frac{2}{3} \cdot \frac{L_0}{S_S\left(r_2^2 - r_1^2\right)}\left(2 + G_S m^4\right) + \frac{1}{S_S} \cdot q \cdot P_2 + \frac{1}{S_S} \cdot q^* \cdot P_1, \qquad \text{(Eq.2-13"')}$$

where r_2 and r_1 are the outermost and the innermost radii of the S2 layer, respectively, and coefficients $\tilde{e}$, $\tilde{q}$ and $\tilde{r}$ are functions of G_u ($=E_u/S_u$) and u ($=u_2/u_1$), and e, q and q^* are functions of G_S ($=E_S/S_S$), θ, and r ($=r_2/r_1$) (See Appendix 1), and P_1 is 0.

Eliminating P_3 from the Eq.2-13' and 2-13", the author obtain the following equation,

$$\begin{aligned}\left(\tilde{e} + 3G_u G_I \tilde{r}\right)\varepsilon_L = {} & \frac{2}{3} \cdot \frac{2 + G_u}{S_u\left(u_2^2 - u_1^2\right)}\left(\tilde{L}_0 + \hat{L}_0\right) + \frac{1}{S_u} \cdot \tilde{q} \cdot P_2 \\ & - \frac{4}{3} \cdot \frac{G_u \cdot \hat{L}_0}{S_u\left(u_2^2 - u_1^2\right)} \cdot \frac{\ln u}{u^2 - 1},\end{aligned} \qquad \text{(Eq.2-14)}$$

provided that the author assumes the continuity of the longitudinal displacement (strain),

$$\hat{\varepsilon}_L = \tilde{\varepsilon}_L = \varepsilon_L$$

To omit the last L_0 terms in the right hand side of Eq.2-14, the following formula is derived (See Appendix 2).

$$G_{\mathrm{u}} \cdot G_I \left(2\varepsilon_{\mathrm{L}} + \hat{\varepsilon}_{\mathrm{T}}\big|_{r=u_2}\right) = \frac{\hat{L}_0}{S_{\mathrm{u}} \cdot u_2^2} \quad . \tag{Eq.2-14'}$$

In this case, ε_{T} should be regarded as the function of r. By substituting the above equation into Eq.2-14, a following equation can be derived:

$$a \cdot \varepsilon_{\mathrm{L}} = b \cdot \hat{\varepsilon}_{\mathrm{T}}\big|_{r=u_2} + \frac{1}{S_{\mathrm{u}}} \cdot p \cdot P_2 + \frac{2}{3} \cdot \frac{2+G_{\mathrm{u}}}{S_{\mathrm{u}}\left(u_2^2 - u_1^2\right)}\left(\tilde{L}_0 + \hat{L}_0\right) \quad , \tag{Eq.2-15}$$

where the coefficients a, b and p are non-dimensional quantities, and they are functions of G_{u}, G_{I} and u (see Appendix 1).

By substituting Eq.2-13''' into Eq.2-15, the author can eliminate the P_2 term, and then the following equation can be obtained.

$$\begin{aligned}\left(a \cdot \frac{q}{S_{\mathrm{S}}} - e \cdot \frac{P}{S_{\mathrm{u}}}\right)\varepsilon_{\mathrm{L}} = {} & b \cdot \frac{q}{S_{\mathrm{S}}} \cdot \hat{\varepsilon}_{\mathrm{T}}\big|_{r=u_2} + \frac{2}{3S_{\mathrm{u}}} \cdot \frac{q}{S_{\mathrm{S}}} \cdot \frac{2+G_{\mathrm{u}}}{\left(u_2^2 - u_1^2\right)}\left(\tilde{L}_0 + \hat{L}_0 + L_0\right) \\ & - \frac{4}{9} \cdot \frac{1}{S_{\mathrm{u}} S_{\mathrm{S}}} \cdot \frac{r_2^2 \cdot L_0}{\left(r_2^2 - r_1^2\right)\left(u_2^2 - u_1^2\right)} B\end{aligned} \tag{Eq.2-16}$$

Coefficient B is described in detail in Appendix 1. It is assumed that an external load $2\pi L$ acts on the wood fiber model along the longitudinal axis, and then can be considered $\tilde{L}_0 + \hat{L}_0 + L_0 = L$.

The unknown variable L_0 is derived as described in Appendix 2. Consequently, Eq.2-16 is rewritten after eliminating the terms of L_0, namely,

$$\begin{aligned}&\left[\left(a \cdot q - e \cdot M \cdot p\right) + \frac{2}{3} M \frac{1}{u^2 - 1} \cdot \frac{B}{2 + G_{\mathrm{S}} \sin^4\theta}\left(e - \frac{1}{4}\left(k^2 - 1\right)q\right.\right. \\ &\times \left\{G_{\mathrm{S}} \sin^2\theta\left(2 - 3\sin^2\theta\right)\left(1 - 2\frac{1}{k^2 - 1}\ln k\right) - 2 - 2G_{\mathrm{S}}\cos^2\theta\sin^2\theta\right\} \left.\left.\right)\right]\varepsilon_{\mathrm{L}} \\ &- b \cdot q \cdot \hat{\varepsilon}_{\mathrm{T}}\big|_{r=u_2} + \frac{1}{3} M \frac{k^2 - 1}{u^2 - 1} q \cdot B \cdot \varepsilon_{\mathrm{T}}\big|_{r=r_2} = \frac{2}{3} \cdot M \cdot q \cdot \frac{2+G_{\mathrm{u}}}{S_{\mathrm{S}} u_1^2\left(u^2 - 1\right)} L\end{aligned} \tag{Eq.2-17}$$

where M=$S_{\mathrm{S}}/S_{\mathrm{u}}$. Three unknown variables, $\varepsilon_{\mathrm{L}}, [\hat{\varepsilon}_{\mathrm{T}}]_{r=u_2}, [\varepsilon_{\mathrm{T}}]_{r=r_2}\left(=[\varepsilon_{\mathrm{T}}]_{r=u_1}\right)$ are contained in Eq.2-17. In this analysis, on the basis of the continuity of the radial displacement, the following boundary condition was imposed on the tangential strains,

$$\varepsilon_T\big|_{r=r_2} = \tilde{\varepsilon}_T\big|_{r=u_1} (\equiv \varepsilon_T^{u1}); \quad \tilde{\varepsilon}_T\big|_{r=u_2} = \hat{\varepsilon}_T\big|_{r=u_2} (\equiv \varepsilon_T^{u2})$$

To solve Eq.2-17, two more equations containing the same unknowns are required. Then the following equations are derived through the solution of Eq.2-12 (in the case of

the S1 layer),

$$\left(r\frac{\mathrm{d}\widetilde{\sigma}_{\mathrm{R}}}{\mathrm{d}r}\right)_{r=u_1} = -\frac{E_{\mathrm{u}}}{2}\left\{1-2\left(\frac{u^2}{u^2-1}\ln u\right)\right\}\cdot\varepsilon_{\mathrm{L}} - 2(P_3-P_2)\frac{u^2}{u^2-1}$$
$$\left(r\frac{\mathrm{d}\widetilde{\sigma}_{\mathrm{R}}}{\mathrm{d}r}\right)_{r=u_2} = -\frac{E_{\mathrm{u}}}{2}\left\{1-2\left(\frac{1}{u^2-1}\ln u\right)\right\}\cdot\varepsilon_{\mathrm{L}} - 2(P_3-P_2)\frac{1}{u^2-1} \qquad \text{(Eqs.2-18)}$$

The P_3-P_2 terms in Eqs.2-18 must be eliminated. P_3 has already been given in Eqn.(A2-1) (see Appendix 2), and P_2 can be obtained from the first equation of Eqs.2-11 (for the S2 layer) and the solution of the differential Eq.2-12 (for the S2 layer). Thereafter, by substituting Eqs.2-18 into the first formula of Eqs.2-11 (for the S1 layer), we obtain the following two equations having $\varepsilon_{\mathrm{L}}, \varepsilon_{\mathrm{T}}^{\mathrm{u1}}$ and $\varepsilon_{\mathrm{T}}^{\mathrm{u2}}$ as unknown variables,

$$\left\{1+2M\frac{u^2}{u^2-1}H+\frac{1}{2}G_{\mathrm{u}}\left(1-2\frac{\mathrm{u}^2}{\mathrm{u}^2-1}\ln u\right)\right\}\varepsilon_{\mathrm{L}}$$
$$+\left\{2+G_{\mathrm{u}}+M\frac{u^2}{u^2-1}\left(k^2-1\right)\left(2+G_{\mathrm{S}}\sin^4\theta\right)\right\}\varepsilon_{\mathrm{T}}^{\mathrm{u1}}+4\frac{u^2}{u^2-1}G_{\mathrm{u}}G_{\mathrm{l}}\varepsilon_{\mathrm{T}}^{\mathrm{u2}}=0 \qquad \text{(Eq.2-19)}$$

and

$$\left\{1+2M\frac{1}{u^2-1}H+\frac{1}{2}G_{\mathrm{u}}\left(1-2\frac{1}{u^2-1}\ln u\right)\right\}\varepsilon_{\mathrm{L}}+M\frac{1}{u^2-1}\left(k^2-1\right)\left(2+G_{\mathrm{S}}\sin^4\theta\right)\varepsilon_{\mathrm{T}}^{\mathrm{u1}}$$
$$+\left(2+G_{\mathrm{u}}+4\frac{1}{u^2-1}G_{\mathrm{u}}G_{\mathrm{l}}\right)\varepsilon_{\mathrm{T}}^{\mathrm{u2}}=0 \qquad \text{(Eq.2-20)}$$

where the coefficient H is described in detail in the Appendix 1. The author can solve the simultaneous Equations 2-17, 2-19 and 2-20 for $\varepsilon_{\mathrm{L}}, \varepsilon_{\mathrm{T}}^{\mathrm{u1}}$ and $\varepsilon_{\mathrm{T}}^{\mathrm{u2}}$.

2.2.4 Longitudinal Young's modulus and the Poisson's ratio of the wood fiber model

The simultaneous Equations 2-17, 2-19 and 2-20, whose unknown variables are $\varepsilon_{\mathrm{L}}, \varepsilon_{\mathrm{T}}^{\mathrm{u1}}$ and $\varepsilon_{\mathrm{T}}^{\mathrm{u2}}$, can be expressed as follows;

$$\begin{bmatrix} a_{11} & a_{12} & a_{13} \\ a_{21} & a_{22} & a_{23} \\ a_{31} & a_{32} & a_{33} \end{bmatrix}\begin{bmatrix} \varepsilon_{\mathrm{L}} \\ \varepsilon_{\mathrm{T}}^{\mathrm{u1}} \\ \varepsilon_{\mathrm{T}}^{\mathrm{u2}} \end{bmatrix} = \begin{bmatrix} \frac{2}{3}\cdot M\cdot q\cdot\frac{2+G_{\mathrm{u}}}{S_{\mathrm{S}}\cdot u_1^2\left(u^2-1\right)}L \\ 0 \\ 0 \end{bmatrix} \qquad \text{(Eq.2-21)}$$

ε_L and ε_T^{u2} are solved as follows;

$$\varepsilon_L = \frac{1}{3}\cdot\left(\frac{A_{11}}{\Delta}\right)\cdot M\cdot q\cdot\frac{2+G_u}{\left(u^2-1\right)}\cdot\frac{u^2}{S_S}\cdot\left(1+\frac{h}{u_2}\right)^2\cdot\bar{\sigma}_l \qquad \text{(Eq.2-22)}$$

$$\varepsilon_T^{u2} = \frac{1}{3}\cdot\left(\frac{A_{13}}{\Delta}\right)\cdot M\cdot q\cdot\frac{2+G_u}{\left(u^2-1\right)}\cdot\frac{u^2}{S_S}\cdot\left(1+\frac{h}{u_2}\right)^2\cdot\bar{\sigma}_l \qquad \text{(Eq.2-23)}$$

where $\bar{\sigma}_l = 2\pi L/(u_2+h)^2$, A_{11}=$a_{22}a_{33}$-$a_{23}a_{32}$, A_{13}=$a_{21}a_{32}$-$a_{22}a_{31}$ and Δ is the determinant of the coefficient matrix in the left hand side of Eq.2-21.

Since h is small enough, ε_T^{u2} is nearly equal to the strain in the diameter of the wood fiber model. Then, the longitudinal Young's modulus E_L and the Poisson's ratio ν_{LT} are written as follows;

$$E_L = \bar{\sigma}_l/\varepsilon_L = 1\Big/\left[\frac{1}{3}\cdot\left(\frac{A_{11}}{\Delta}\right)\cdot M\cdot q\cdot\frac{2+G_u}{\left(u^2-1\right)}\cdot\frac{u^2}{S_S}\cdot\left(1+\frac{h}{u_2}\right)^2\right] \qquad \text{(Eq.2-24)}$$

$$\nu_{LT} = -\varepsilon_T^{u2}/\varepsilon_L = -A_{13}/A_{11} \qquad \text{(Eq.2-25)}$$

Based upon above theory, the author writes a N88-BASIC program. The program used by the simulation is shown in Appendix 3.

2.2.5 Determining the parameter values in the equations

To calculate the values of E_L and ν_{LT} by using formulae 2-24 and 2-25, the author has to give proper values to the parameters, E_u, E_S, S_l, S_u, S_S, u, k, h, and θ whose meanings are defined in Nomenclature.

According to the method employed in the previous study (Yamamoto et al.2001), the axial Young's modulus of the cellulose crystal E_{cry}, the isotropic Young's modulus of the matrix substance E_{matr}, and the weight ratio of the cellulose crystal to the matrix substance in each cell wall layer are important factors for determining the values of E_u, E_S, S_l, S_u, and S_S. It is generally considered that E_{matr} varies with the moisture content change, however, E_{cry} is not affected by the moisture adsorption. Srinivasan (1941) and Cousins (1976,1978) revealed that the Young's modulus of the molded matrix substance takes a value of 2GPa above the fiber saturation point (FSP), then, it increases monotonously depending on the water desorption, and it reaches values of 4-6GPa at the oven-dried state. Then, in this study, as the standard value for E_{matr}, of 2GPa is adopted above the FSP, and of 4GPa at the oven-dried state. Moreover, the author

supposes that moisture content dependency of E_{matr} is following a sigmoidal curve with reference to a previous report (Yamamoto et al. 2001)

The framework of the CMF is composed of the rigid crystal which is not affected by the moisture sorption. Then, we suppose the 134GPa as the standard value of E_{cry} with reference to Sakurada et al. (1962) and Nishino et al. (1995). On the other hand, Ishikawa et al (1997, 1998) tried to estimate the Young's modulus of the amorphous cellulose by using ramie fiber, and they determined it 4-8GPa in air-dried condition. Then, in this study, it is assumed that the amorphous region in the CMF behaves as matrix substance for convenience.

Regarding the distribution of the chemical components within the wood cell wall, it should be considered that it is highly dependent on species and age of the wood. In calculating the elastic properties of the wood by using Eq.2-24 and 2-25, the weight ratio of the cellulose crystal to the matrix substance is applied within a range of values so as to simulate the observable phenomena quantitatively. Thus, the author can determine the values of E_u, E_S, S_I, S_u, and S_S.

The values of the parameters u, k and h are estimated by the formulae on the relationships between the density of the specimen and the volume ratios of layers to the whole cell wall (Yamamoto et al. 2001). Those parameters also depend on the moisture content, however, their changes due to the moisture adsorption are so small as to be neglected compared to that E_{matr}.

2.3 Case studies and discussions

2.3.1 MFA dependency of the longitudinal Young's modulus

Many researchers have reported that the longitudinal Young's modulus of the small coniferous wood specimen tends to decrease as the MFA in the S2 layer increases (Cave 1968, Sobue and Asano 1976). Their conclusions were confirmed also by the experimental using an isolated softwood fiber (Page et al. 1977). Furthermore, many researchers have tried to explain its origin by using the theoretical models having unidirectionally reinforced cell walls (Cave 1968, 1978a, 1978b, Sobue and Asano 1976, Salmen 1982, Salmen and De Ruva 1985, Koponen 1991, Norimoto et al. 1967). Then, based upon the wood fiber model introduced in this study, it is tried to simulate the MFA dependency of the substantial Young's modulus of the wood in the longitudinal direction E_L^W, which is defined as follows:

$$E_L^W = E_L \cdot \frac{\rho^W}{\rho_0} \qquad \text{(Eq.2-26)}$$

where ρ^W is the density of the cell wall, and ρ_0 is the density of the wood in the oven-dried condition. When using the formulae 2-24 and 2-25, the weight ratio of the cellulose crystal to the matrix substances is assumed as shown in Table2-2.

Simulated results were plotted with the observed ones in Fig.2-4. The observed ones were obtained at the air-dried condition (20-25°C, 50-65%RH), and the simulated results were given under the assumption that the moisture content of the wood fiber model is 12%. Figure2-4 demonstrates that the observed results can be quantitatively simulated when the ratio of the cellulose crystal to the matrix substance in each layer is chosen adequately, which suggests that the elastic properties of the wood can be formulated on the basis of the reinforced-matrix hypothesis.

From Fig.2-4, it becomes apparent that the relationship between the MFA and E_L^W is dependent on tree species. Regarding the dependency of the relationship between the MFA and E_L^W on species origin, the following possibilities (1), (2) and (3) can be referred to:

(1) The ratio of the cellulose crystal to the matrix substance is different among species, or between the mature wood and juvenile wood in the same trunk. This is a problem

concerning the biosynthesis of the secondary xylem.

(2) Crystallinity of the cellulose microfibril tends to vary with time, which changes the ratio of the cellulose crystal to the matrix substance. This presents a problem regarding the time dependent properties of the materials after lumbering.

(3) Drying and heating processes give an irreversible change to the cohesion state of each cell wall component as pointed out by Furuta et al. (1998). In such cases, the value of the Young's modulus of the matrix substance (E_{matr}) would change from the original value.

At present, the probabilities of the above-mentioned possibilities (1), (2) and (3) cannot be examined, since the author has no information on the sampling positions and ages of the materials used for the experiment in Fig.2-4. Thus, a proper experiment needs to be planned in order to make clear which possibility among (1), (2) and (3) is the most reasonable.

2.3.2 Moisture content dependency of the longitudinal Young's modulus

It is well known that the longitudinal Young's modulus of the wood (E_L) tends to decrease with an increase in the moisture content. This decrease is often up to 30-40% of the oven-dried Young's modulus. Above FSP, on the other hand, it is more or less constant (Kollmann and Krech 1960).

It is generally believed that the reduction in Young's modulus of the wood due to the increase of the moisture content is caused mainly by the hygrosoftening of the matrix substance which is an isotropic mixture of lignin, hemicellulose. Amorphous region in the CMF is also important. Because of its nature, it is highly sensitive to the moisture changes. Then, in this section, based on Eq.2-24, the author tries to verify the above-mentioned explanation.

E_L in Eq.2-24 is controlled by various parameters, and some parameters are dependent on the moisture content. In this study, the author examines the effect of the moisture content in the cell wall upon the value of E_L, and then adopts 2GPa, 4GPa and 134GPa as the standard values for E_{matr} at FSP, the oven-dried state and for E_{cry}, respectively. Moreover, as value of E_{matr} at the oven-dried condition, various values besides 4GPa are assumed, and thus the relationship between E_L and the moisture content is calculated.

The weight ratio of the cellulose crystal to whole substance in each layer of the secondary wall is supposed to be 40% in the S2 layer and 20% in the S1 layer.

The simulated results are shown in Fig.2-5. Dots represent experimental data of spruce specimens whose density is 0.52g/cm^3 (Kollmann and Krech 1960). Moreover, the MFA in the S2 layer of the experimental specimen had been left unknown. However, considering the specimen used in Fig.2-5 is composed of sufficiently matured tracheids, 10degrees as the MFA may be assumed when calculating Eq.2-24. To obtain a reasonable simulation, E_{matr} was assumed to be from 24-28GPa at the oven-dried state, which is rather larger as compared to the standard value of 4GPa. Accepting both Cousins' (1976,1978) experiments and the reinforced-matrix hypothesis, one cannot help regarding this result as an unreasonable crux. As the origin of such crux, the following possibilities (1), (2) and (3) are referred to:

(1) Inside the actual wood cell wall, E_{matr} takes on value of 2GPa at the FSP, however, it takes several times as large a value as that of isolated matrix substance at the oven-dried condition.

(2) Inside the actual wood cell wall, E_{matr} takes on several times as large a value as that of isolated matrix substance not only at the oven-dried condition but also within a large range of the moisture content. However, if the properties of the compound middle lamella (CML) vary with the water sorption, then shear or slipping deformations will be caused between adjoining fibers by the tensile load. Thus, E_L becomes considerably small with increasing the moisture content.

(3) Inside the actual wood cell wall, E_{matr} takes on values of 2GPa at FSP, and 4GPa at oven-dried condition. On the other hand, the CMF framework as a bundle becomes more stiff as the moisture content decreases.

In this stage, it is not sure which possibility holds, however, an experiment can be proposed so as to verify possibility (1). If this would be the right one, the reduction of the E_L due to the water sorption should become more remarkable in specimen with large MFA than in the one with small MFA, which was pointed out theoretically by Salmen (1982).Therefore, it is planned to examine the possibility (1) through an experiment using samples prepared from normal wood and compression wood or juvenile wood having a large MFA. The details of this experiment were discussed in Chapter 3.

It is quite difficult to admit possibility (2) because of the following reasons: First, the wood can be regarded as a continuous parallel fiber lamina consisting of numerous tracheids, thus, it is expected that the contribution of the elastic modulus in the CML to E_L becomes quite small according to the simple rule of mixture (Mallick 1988). Second, if shear or slipping deformation would occur in the CML between adjoining fibers at high moisture content, the author expects that many tracheids would have pulled out from one another along the CML when the specimen was broken in tension. On the basis of the scanning electron microscopic observation, Saiki (1973) revealed that separation of the tracheid frequently seems to occur along the CML in the late-wood zone, on the other hand, failure in the early-wood zone takes the form of brittle tension with separation occurring across the cell walls. Moreover, several researchers, including Saiki (1973), have demonstrated that what appeared to be a failure in the CML was actually a failure in the outer region of the secondary wall even in the case of high moisture content (e.g. Mark 1967).

As to the possibility (3), it appears a little strange since the CMF crystal would not react with the water molecule. Then, to discuss this possibility while still accepting 4GPa as the standard value of E_{matr} at the oven-dried state, the following hypothesis is assumed on the mechanical property of the wood CMF framework:

From a mechanical point of view, there is an intermediate domain between rigid crystal and completely disordered amorphous domains in the wood CMF bundle, and such a domain fluctuates between quasi-crystal and quasi-amorphous states in accordance with the moisture adsorption. The quasi-crystal domain, which is mechanically close to the complete crystal domain, tends to increase with water desorption. Therefore, the axial Young's modulus of the CMF as a bundle tends to increase as the moisture content decreases. Transformation from quasi-amorphous to quasi-crystal states may be more or less reversible. This is a main reason why the longitudinal Young's modulus of wood becomes larger with drying.

Based on this idea, the moisture dependency of the E_L was simulated. Results are shown in Fig.2-6. A reasonable simulation is obtained assuming that the content of the unstable domain in the secondary wall reaches about one-third as much as the content of the stable crystal domain. This result is also effective for simulating the behavior of

specimens with densities other than 0.52g/cm^3 (Fig.2-7).

Salmen (1982) pointed out a possibility that a hygroplaticization occurs in the disordered regions of the CMF of the wood pulp fiber, and successfully explained the drastic reduction of the elastic modulus of the wood pulp fiber or the paper when it is immersed in water. At the same time, he proposed the laminate model of the infinite plane cell wall, and he showed that the observed reduction of E_L in the wood fiber due to moisture adsorption can be predicted by the softening of the hemicellulose (Salmen 1982, Salmen and De Ruvo 1985, Salmen et al. 1985). Then, he deduced that no noticeable hygroplasticization due to water impregnation takes place in the CMF of wood cell wall. However so far as using the wood fiber model introduced in the present study, it should be rather considered that water impregnation causes a certain hygroplaticization in the CMF framework of wood cell wall. It is natural to consider that a drastic hygroplasticization occurs in the unstable domain, which should be distinguished from stable amorphous domain-namely, permanently amorphous cellulose, hemicellulose, and their mixture.

Recently, Tokoh et al. (1998) observed that the cellulose microfibrils of *Acetobacter xylinum* formed in medium containing acetyl glucomannan are loosely arranged in contrast to the stiff ribbon-like fibrils formed in the controlled medium. Further, they noticed that with the glucomannan, droplet-like structures of hemicellulose are developed around the base of the microfibrils. It was therefore concluded that the deposition of the matrix substance, e.g. hemicellulose, into the CMF aggregates would not only induce the stability of the bundle but also assist in the formation of the heterogeneous configuration in the bundle.

Referring to Tokoh's report, the author images the CMF structure in the wood cell wall visually as showing in Fig.2-8. The CMF framework in the secondary wall forms a structure based on the "stripe lamella hypothesis" proposed by Kataoka et al. (1992). Then, if it was formed as a bundle of several units of the wood CMF (CMF aggregation), the image at the electron microscope level would be illustrated as shown in Fig.2-8a. The matrix substances, mainly hemicellulose, which deposits later than the CMF deposition, are not only filling up pore space between the CMF aggregations but also penetrating in the CMF aggregations. As a result, it is considered that the crystallinity

was blocked and stable amorphous region was made near part of the penetrated matrix substance as shown in Fig.2-8b. On the other hand, the unstable domain was formed around the amorphous region, which takes a mixed structure of both quasi-crystal state and quasi-amorphous state, and the ratio of both states may be dependent on the moisture. The author images that the stable amorphous region distributes like a jigsaw puzzle at the surface of the CMF aggregations, and the unstable domains spread around the each jigsaw puzzle-like amorphous region.

2.4 Conclusion

In this chapter, the longitudinal Young's modulus of the isolated wood fiber was formulated on the basis of the reinforced-matrix hypothesis.

Some case studies on the elastic properties of the wood were given using the newly-derived model. As a result, some hypotheses on the microscopic properties of the cell wall constituents peculiar to the wood were predicted.

The hypotheses given in this chapter were examined and verified in the next chapter (Chapter 3).

2.5 Summary

In this chapter, the author tries to predict the origin of the longitudinal Young's modulus of the clear wood specimen in relation to the composite structure of the wood cell wall. Then, an analytical procedure was developed on the basis of the idea of "the reinforced-matrix hypothesis" originally introduced by Barber and Meylan (1964).

A multi-layered circular cylinder, having the CML, the S1 and the S2 layer, was used as a model of the ligno-cellulosic (wood) fiber, and the elastic properties of an isolated wood fiber were formulated mathematically. In the formulation, not only the structural factors, such as the microfibril angle and the thickness of each layer, but also the environmental condition, e.g. the moisture content, were taken into consideration.

The effects of the moisture content and the microfibril angle upon the longitudinal Young's modulus of the wood fiber were simulated by using the newly derived formulae. It is anticipated to give a start to estimate the fine structure and the internal properties of the cell wall constituents in relation to the macroscopic behaviors of the wood through simulating the mechanical behaviors of the wood fiber.

Figures and Tables in Chapter 2

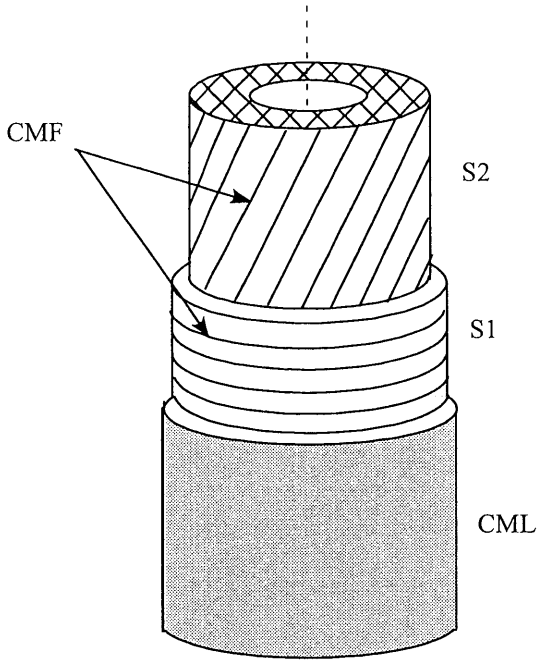

Fig.2-1. Wood fiber model-three layered wood fiber (Tracheid).

CMF; cellulose microfibrils. S1; the outer layer of the secondary wall. S2; the middle layer of the secondary wall. CML;Compound middle lamella.

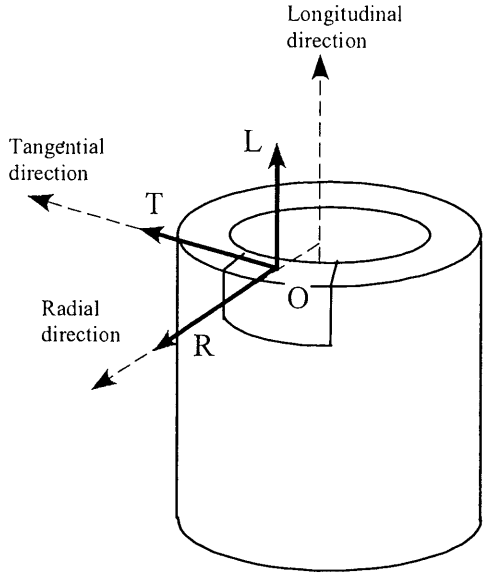

Fig.2-2. L,T,R local orthogonal coordinate.

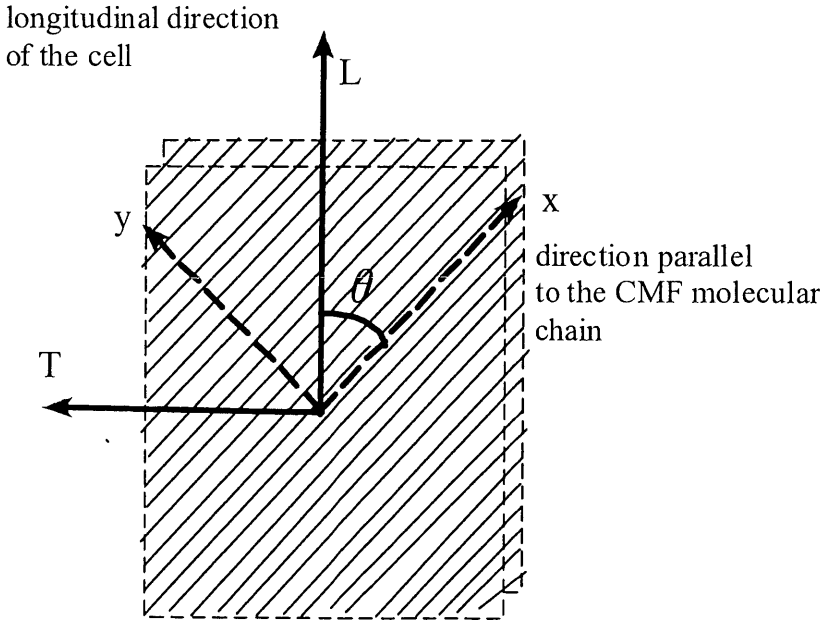

Fig.2-3. Flat-board of the CMF bundle.

Table2-1. Correspondence of the symbols to various parameters in the equations.

	θ	r_{in}	r_{out}	r $(=r_{out}/r_{in})$	S	E	P_{in}	P_{out}	L_0	α	ϕ	φ
CML	---	u_2	u_2+h	$\frac{u_2+h}{u_2}$	S_l	0	P_3	0	$\hat{L}_0$	1	---	$-\frac{u_2}{3h}$
S1	90	u_1 $(=r_2)$	u_2	u	S_u	E_u	P_2	P_3	$\tilde{L}_0$	$\tilde{e}$	$\tilde{r}$	$\tilde{q}$
S2	θ	r_1	r_2	k	S_S	E_S	0	P_2	L_0	e	q	q^*

Table2-2. Weight proportion (%) of CMF crystal to the matrix substance in each layer of typical early-wood tracheid.

	(Case 1)		(Case 2)		(Case 3)		(Case 4)	
	CMF	MT	CMF	MT	CMF	MT	CMF	MT
CML	15	85	15	85	15	85	15	85
S1	12	88	18	82	24	76	30	70
S2	24	76	37	63	48	52	60	40
S3	---	---	---	---	---	---	---	---

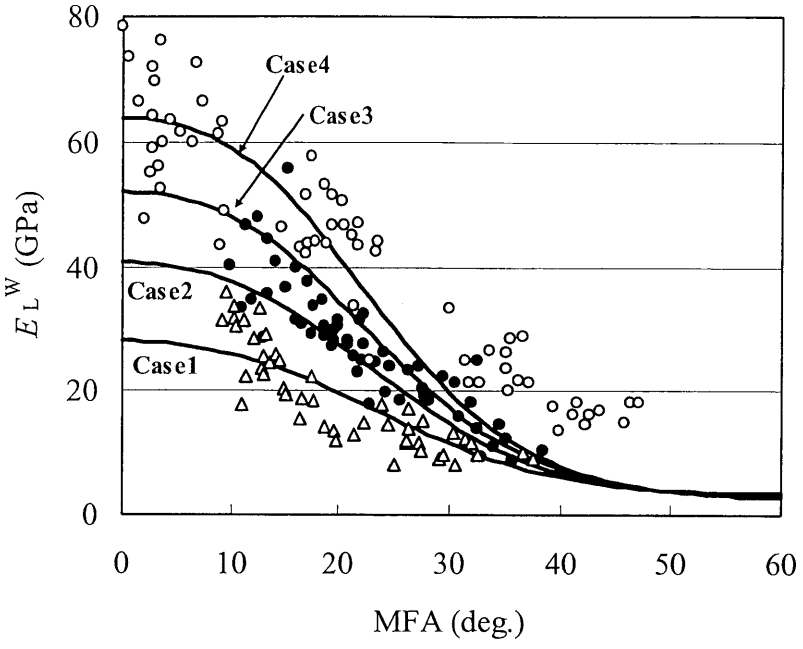

Fig.2-4. Relationships between substantial Young's modulus of the wood (E_L^W) and the MFA.

○; An isolated holocellulose fiber of *Spruce sp.* (Page et al. 1977).

●; A thin specimen of *Pinus radiata* (Cave 1968).

Δ; A thin specimen of Sugi (*Cryptomeria japonica*, Sobue and Asano 1976).

All experimental results were obtained under air-dried condition.

Conditions for simulation:

1) The assumed weight ratio of the cellulose crystal to the matrix substance in each layer is listed in Table2-2.
2) E_{matr} tends to increase monotonously from 2GPa at the fiber saturation point to 4GPa at the oven-dried state.
3) Average moisture content of the cell wall is 12%.

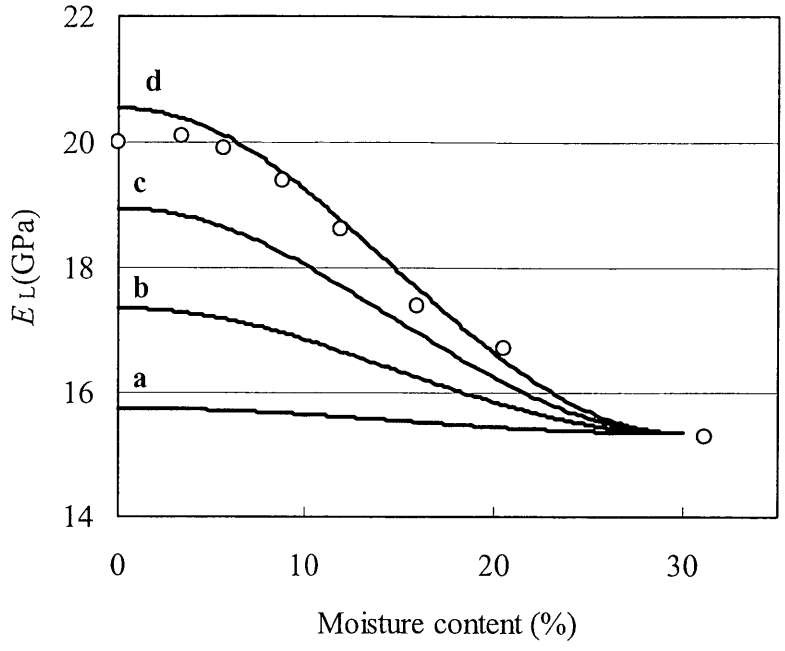

Fig.2-5. Moisture content dependency of the longitudinal young's modulus of the wood (E_L).

Experimental results are obtained from a wood specimen of spruce (density 0.52g/cm^3, Kollmann and Krech 1960).

Conditions for the simulation:

1) The weight ratio of the cellulose crystal to whole substance in each layer of the secondary wall is 40% (S2), and 20% (S1).
2) E_{matr} tends to increase monotonously from 2GPa at the fiber saturation point to **a**; 4GPa, **b**; 12GPa, **c**; 20GPa, **d**; 28GPa at the oven-dried state.
3) MFA in the S2 layer is 10 degree.

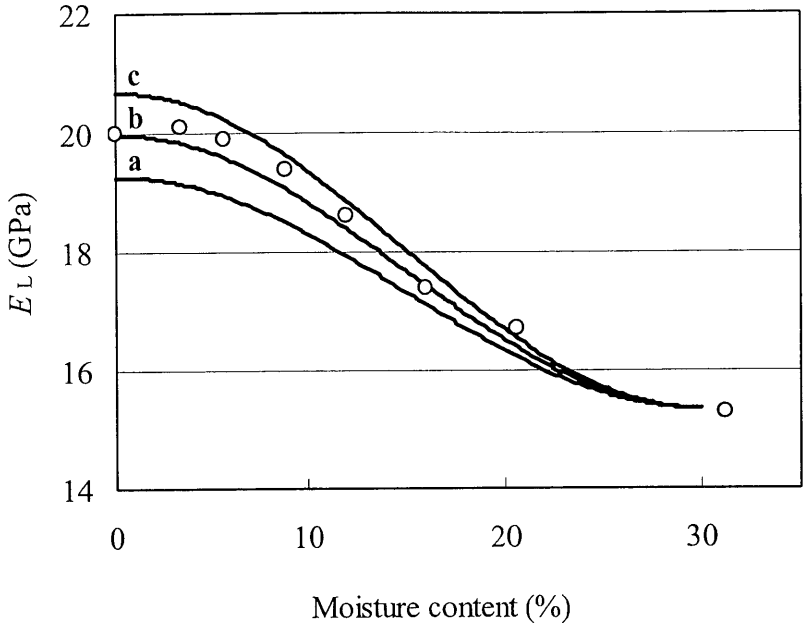

Fig.2-6. Moisture content dependency of the longitudinal Young's modulus of the wood.

1) In this case, it is supposed that the CMF contains unstable domain which changes from compliant quasi-amorphous state to rigid quasi-crystal state in accordance with moisture sorption.
2) Experimental results are obtained from a wood specimen of spruce (density 0.48g/cm^3, Kollmann and Krech 1960).

Conditions for the simulation:

1) The weight ratio of the cellulose crystal to whole substance in each layer of the secondary wall is 40% (S2), and 20% (S1).
2) The weight ratio of the unstable domain to whole substance in each layer of the secondary wall is: **a**; 10% (S2), 5% (S1) **b**; 12% (S2), 6% (S1) **c**; 14% (S2), 7% (S1).
3) E_{matr} tends to increase monotonously from 2GPa at the fiber saturation point to 4GPa at the oven-dried state.
4) MFA in the S2 layer is 10 degree.

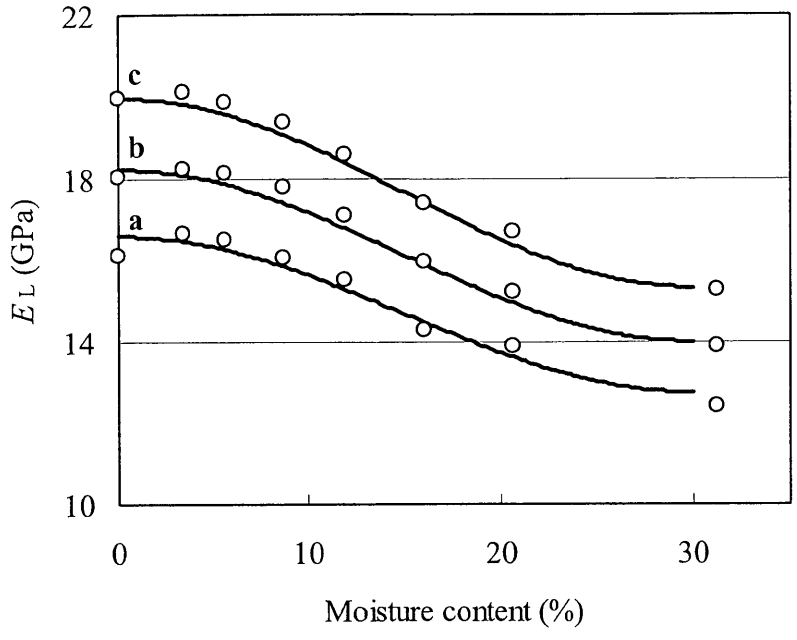

Fig.2-7. Moisture content dependency of the longitudinal Young's modulus of the wood.

1) In this case, it is supposed that the CMF contains unstable domain which changes from compliant quasi-amorphous state to rigid quasi-crystal state in accordance with moisture sorption.
2) Experimental results are obtained from a wood specimen of spruce (density, **a**; 0.44g/cm^3 **b**; 0.48g/cm^3 **c**; 0.52g/cm^3, given by Kollmann and Krech 1960).

Conditions for the simulation:

1) The weight ratio of the cellulose crystal to whole substance in each layer of the secondary wall is 40% (S2), and 20% (S1).
2) The weight ratio of the unstable domain to whole substance in each layer of the secondary wall is: 12% (S2), 6% (S1).
3) E_{matr} tends to increase monotonously from 2GPa at the fiber saturation point to 4GPa at the oven-dried state.
4) MFA in the S2 layer is 10 degree.

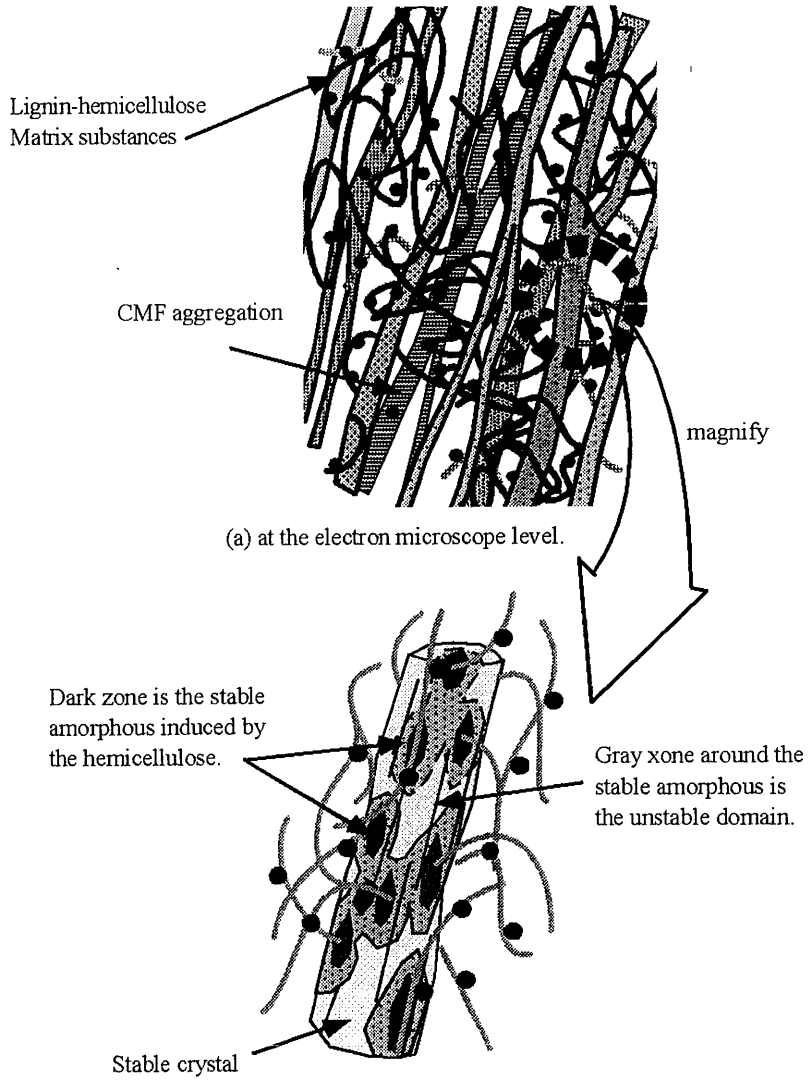

Fig.2-8. An image of the microstructure of the wood cell wall.

a; at the electron microscope level. b; interface of the CMF and the matrix.

CHAPTER 3 ORIGIN OF THE MOITURE DEPENDENCY OF THE LONGITUDINAL ELASTICITY OF WOOD

3.1 Introduction

In the previous chapter (Chapter 2), perceiving the multi-layered circular cylinder model consisting of the compound middle lamella (CML), the S1 layer and the S2 layer, the author formulated the longitudinal Young's modulus of an isolated wood fiber that was predicted in relation to the microfibril angle (MFA) and the moisture content. To explain quantitatively the fact that the longitudinal Young's modulus of wood (E_L) tends to increase as the moisture content decreases, the author developed two hypotheses on the behavior of the cell wall constituents.

The first attributes the moisture dependency of E_L to the matrix substance (Norimoto and Yamada 1967). In a simulation using the wood fiber model, this implies that the Young's modulus of the matrix substance (E_{matr}) under oven-dried condition is several times larger than that at the fiber saturation point (FSP). According to Cousins' (1976, 1978) experiments, the Young's modulus of the isolated matrix substance is only two or three times larger than that at the FSP.

The second holds that there is an intermediate (unstable) domain between the rigid crystal and the compliant disordered amorphous domains in wood CMF bundle. This domain fluctuates between the crystal-like and the amorphous-like states, at which the elastic modulus is of the same order as the lignin-hemicellulose matrix in accordance with moisture adsorption. The crystal-like state, which is mechanically similar to the complete crystal domain, tends to increase with water desorption. Therefore, the axial Young's modulus of the CMF as a bundle tends to increase as the moisture content decreases. Thus, E_L becomes larger with drying. As mentioned in the previous chapter, this hypothesis is based on the studies reported by Cousins (1976, 1978) on the relationship between the elastic modulus of the isolated matrix substance and its moisture content. However, since the results of Cousins (1976, 1978) were obtained from the isolated matrix substance, the author cannot ignore the first hypothesis.

This chapter discusses the moisture dependency of E_L using experimental results of the tensile test using a small clear specimen of sugi (*Cryptomeria japonica* D.Don) and

simulations using the wood fiber model. Then, the author determined which of the two hypotheses is valid.

3.2 Material and Methods

3.2.1 Materials

A-25-year-old, 20-cm DBH sugi (*Cryptomeria japonica* D.Don) growing in Nagoya university experimental forest was used as the materials.

3.2.2 Sample preparation

Four blocks (A, B, C, D) of normal wood were cut from the sapwood and the outer most region of the heartwood. Two blocks (E, F) were cut from the juvenile wood. Each block was about 70×8×50mm in L×T×R directions, respectively. After cutting the blocks, they were boiled in hot water for 5minutes, three times, to saturate them. Then, tangential sections 0.2mm thick were prepared from the early-wood region of each block using a sliding microtome and used for the tensile test. Small blocks for measuring the oven-dried density were cut from the same annual rings as the specimen used for the tensile test.

3.2.3 Methods

(a) Longitudinal Young's modulus Measurement

To prevent slippage at the clamps during tensile test, pieces of sandpaper were attached to each edges of specimen using quick-drying glue. Then, the specimen were put in an air-conditioned cabinet. The moisture content of the specimen was controlled using H_2O, NaCl aq, Silica Gel, and P_2O_5 powder, at 100%, 76%, 20~23% and 0% RH at 20°C, respectively. The test was conducted in an air-conditioned room at 20°C. After the specimen reached each equilibrium moisture content, they were attached to the hand-made testing machine with an air-conditioned system (Fig.3-1). Two spots 20~30mm apart along the grain were marked with black enamel paint to measure the displacement caused by the tensile load. To measure the distance between the two dots, a traveling microscope with an xy-microstage (0.001mm accuracy) was used. Then, a stress-strain curve was obtained and used to calculate the longitudinal Young's modulus. Tensile tests were performed in the wet state in addition to the four RH conditions. For each RH condition, five specimen were used for the tensile test.

(b) Microfibril angle determination

After the tensile test was performed, the microfibril angle (MFA) in the S2 layer of each specimen was measured using an X-ray diffractometer (Shimadz, XD-D1w type) (Yamamoto et al. 1993).

(c) Wood density measurement

Wood density was determined by the gravimetrical method using mercury impregnation. The wood density of each specimen was determined after small specimen prepared reaching constant weight in an oven at 105°C for 24 hours. To measure oven-dried volume, the mercury displacement technique was employed.

(d) Simulation using a wood fiber model

The formulation derived in the previous chapter (Chapter 1) was used in this chapter. The formula (Eq.2-24) which predicts the longitudinal Young's modulus of the wood fiber is characterized by several parameters, which represent the structure and mechanical/physical properties of the lignified cell wall. Those were listed in Table2-1 (in Chapter 2).

In this chapter, measured MFA was used for the simulation. Thickness in each layer was estimated from the measured oven-dried density and the formula derived in the previous study (Yamamoto et al. 2001). In case of using this formula, the volume ratios of layers to the whole cell wall layer should be given in advance. In this simulation, the author used the data on the typical early-wood tracheid given by Koponen et al. (1989).

Ratio of the cellulose crystal to the whole substance in each layer determines the mechanical rigidity in the CMF framework as the bundle and the lignin-hemicellulose as a matrix. The ratio was assumed on a case-by case basis in the simulation. In this simulation, the author used the value of 134GPa as the Young's modulus of the cellulose crystal in the direction parallel to the molecular chain (Sakurada et al. 1962, 1964). On the other hand, the author assumed that the non-crystalline polyose including the amorphous cellulose is mechanically equivalent to the matrix substance.

3.3 Results and Discussion

Table 3-1 shows the MFA and oven-dried density of the specimen. Blocks A to D were prepared from mature (normal) wood, and both the MFA and density were comparatively low. On the other hand, the values for blocks E and F were quite high, since they were prepared from juvenile wood. Then, the author discusses the moisture dependency of E_L in relation to the MFA. Figs.3-2 show the relationships between the moisture contents and E_L. The points are the experimental results. As observed in these figures, E_L tended to decrease as the moisture content increased below the FSP, and it becomes constant above the FSP. These observations concur with various experimental reports (e.g. Kollmann and Krech 1960). The percentage reduction of E_L from the oven-dried state to the FSP tended to be constant or slightly decrease as the MFA increased. Figure 3-3a shows that E_L decreased as the MFA increased for each RH condition. Moreover, Fig.3-3b shows the relationship between the substantial Young's modulus (E_L^W) and the MFA. E_L^W is defined as Eq.2-26 in Chapter 2.3. Figures 3-3 and 3-4 show the relationship between the MFA and the percentage reduction of E_L due to water sorption more visually than Figs.3-2.

Here, the author examines the hypothesis that the reduction in E_L due to water sorption is dominated mainly by the moisture properties of the matrix substance. According to this hypothesis, inside the actual wood cell wall, E_{matr} takes a value of 2GPa at the FSP, and is several times greater than the value for isolated matrix substance under oven-dried condition. If this is correct, the reduction of E_L due to water sorption should be more remarkable in specimen with a large MFA than in those with a small MFA. This is quite natural, since E_L is dominated mainly by the matrix substance at a large MFA, while is dominated mainly by the CMF at a small MFA. As can be observed in Figs.3-3 and 3-4, however, the reduction of E_L tends to increase slightly in specimen with a small MFA than in those with a large MFA, or to be almost constant regardless of the MFA. The solid lines in Fig.3-4 indicate the simulated results using the wood fiber model, in which the author assumes that the values of E_{matr} in the oven-dried state are 4, 7 and 10GPa. Those values were based on the assumption that the moisture dependency of E_L is due only to that of the matrix substance. Discrepancy between experimental results and the predicted ones were rather remarkable especially in the

specimen with a large MFA. This result is thought to rule out the first hypothesis.

Next, the author assumes that the value of E_{matr} inside the actual cell wall is as large as that of isolated matrix substance. Referring to Cousins (1976, 1978), the author used 2 and 4GPa as the standard value for E_{matr} at the FSP and the oven-dried condition, respectively. The author hypothesized that there is an intermediate (unstable) domain between the rigid crystal and the compliant disordered amorphous domain in the wood CMF bundle. Moreover, this domain fluctuates between quasi-crystal and quasi-amorphous states in accordance with moisture adsorption. The quasi-crystal domain, which is mechanically similar to the complete crystal domain, tends to increase with water desorption; therefore, the axial Young's modulus of the CMF as a bundle tends to increase as the moisture content decreases. Based upon this hypothesis, the author simulated the moisture dependency of E_L measured in sugi. The results are shown in Figs.3-5. The condition imposed in each simulation was shown in Table 3-2. For small MFAs, reasonable simulations are performed when suitable values are given for the content of the intermediate (unstable) domain in the CMF bundle. On the other hand, the unstable domain in the CMF bundle appears to have less effect on the E_L for large MFAs. This concurs with the fact that E_L is markedly affected by the matrix substance for large MFAs, while it is affected by the CMF crystal framework for small MFAs. Therefore, the second hypothesis is supported in this stage.

3.4 Conclusion

In the previous chapter (Chapter 2), the author proposed two hypotheses that explain the origin of the moisture dependency of the longitudinal Young's modulus of wood. In this chapter, the author examined their consistencies on the basis of the experiment and theoretical calculation. As a result, the author concludes that the new hypothesis, which hypothesizes an intermediate (unstable) domain between the rigid crystal and the compliant disordered amorphous domains in wood CMF bundle, is more consistent with the observed phenomena. This intermediate domain fluctuates between the crystal-like and the amorphous-like states in accordance with moisture adsorption. The author needs to verify this hypothesis through further investigation.

3.5 Summary

This chapter examined the origin of the moisture dependency of the longitudinal Young's modulus of wood (E_L) in relation to the microfibril angle (MFA) of the S2 layer of the secondary wall. Microtomed early-wood specimen of sugi (*Cryptomeria japonica* D.Don) were used for the experiment. The following was revealed:

(1) E_L tends to decrease as the moisture content increases in the region below the fiber saturation point (FSP).

(2) The percentage reduction of E_L from the oven-dried state to the FSP tends to increase slightly in specimen with a small MFA than in those with a large MFA, or to be almost constant regardless of the MFA.

Subsequently, the relationship between E_L and the moisture content was simulated theoretically using the simplified wood fiber model proposed in the previous chapter (Chapter 2). The simulation considered the two hypotheses proposed in Chapter 2 for the origin of the moisture content dependency of E_L. The first is a traditional theory that the reduction of E_L is caused mainly by the moisture dependency of the lignin-hemicellulose matrix. The second assumes that an intermediate domain exists between the rigid crystal and the compliant disordered amorphous regions in wood cellulose microfibril (CMF). It is assumed that such a domain fluctuates between the rigid quasi-crystal and the compliant quasi-amorphous states at which the elastic modulus is of the same order as the lignin-hemicellulose matrix in accordance with the moisture sorption.

When the first hypothesis is adopted for the simulation, the percentage reduction of E_L from the oven-dried state to the FSP should increase as MFA increases; this was contradicted by the experimental results (2). On the other hand, when the second hypothesis is applied to the simulation, the experimentally obtained results (1) and (2) are simulated reasonably. This suggests that the moisture dependency of E_L is controlled by the second hypothesis.

Figures and Tables in Chapter 3

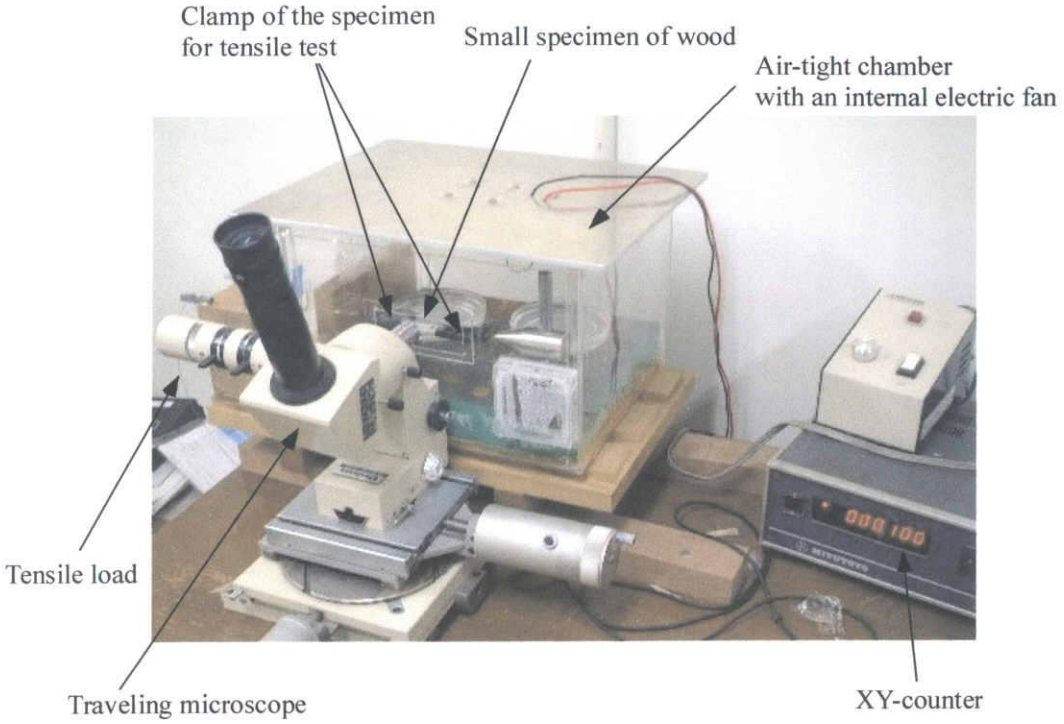

Fig.3-1. The hand made tensile testing machine set.

Table 3-1. The average values of MFA and oven-dried density for blocks A to F.

Specimen	A	B	C	D	E	F
MFA (deg.)	10.6	14.0	20.6	25.8	31.4	36.6
density (g/cm^3)	0.21	0.22	0.26	0.29	0.31	0.22

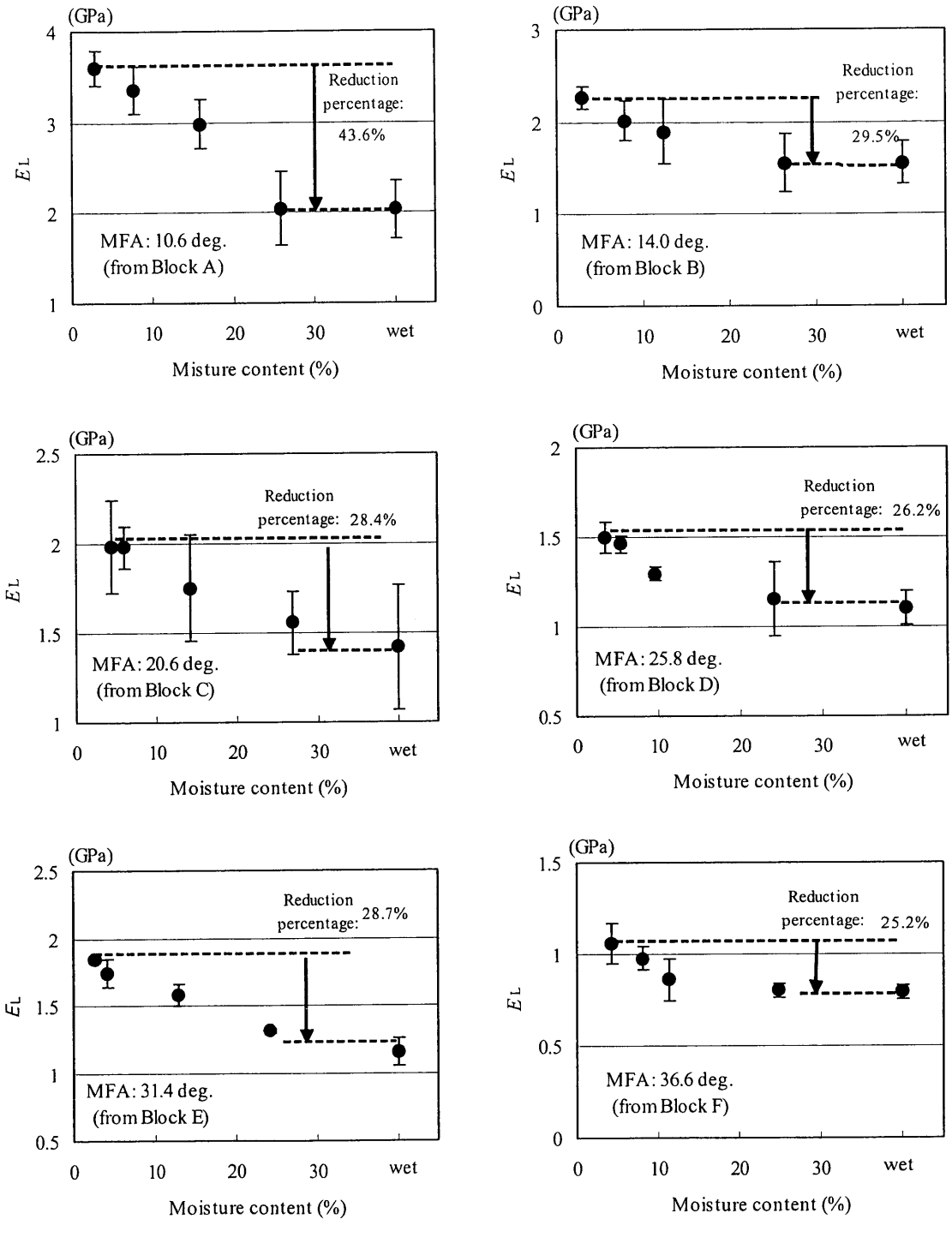

Figs.3-2. Moisture content dependencies of the longitudinal Young's modulus of the wood (E_L).

Note:

1) Each plot represents an average value.

2) The error bar represents the standard deviation.

3) The specimen was cut from block A~F (See Table 3-1).

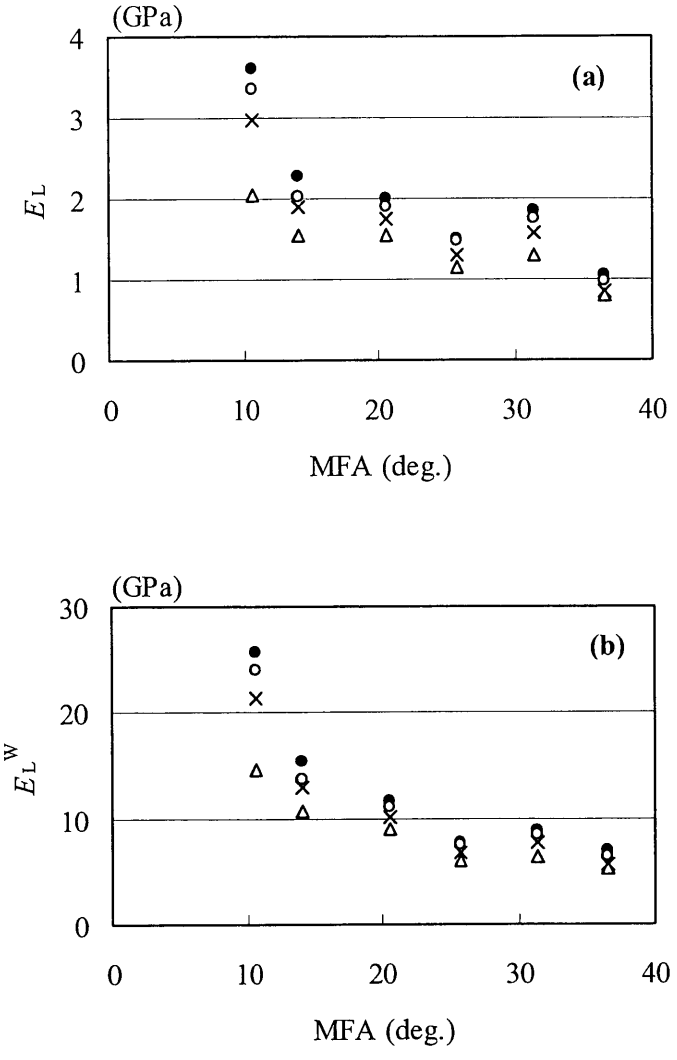

Figs.3-3. The relationships between the longitudinal Young's modulus of the wood (E_L), the substantial longitudinal Young's modulus of the wood (E_L^W), and the MFA.

Legends: ●; 0%RH (conditioned by P_2O_5 powder), ○; 20~23%RH (by Silica Gel grain), ×; 76%RH (by NaCl aq.), Δ; 100%RH (by H_2O).

Note: All the experimental results were obtained from a small sugi specimen at 20°C.

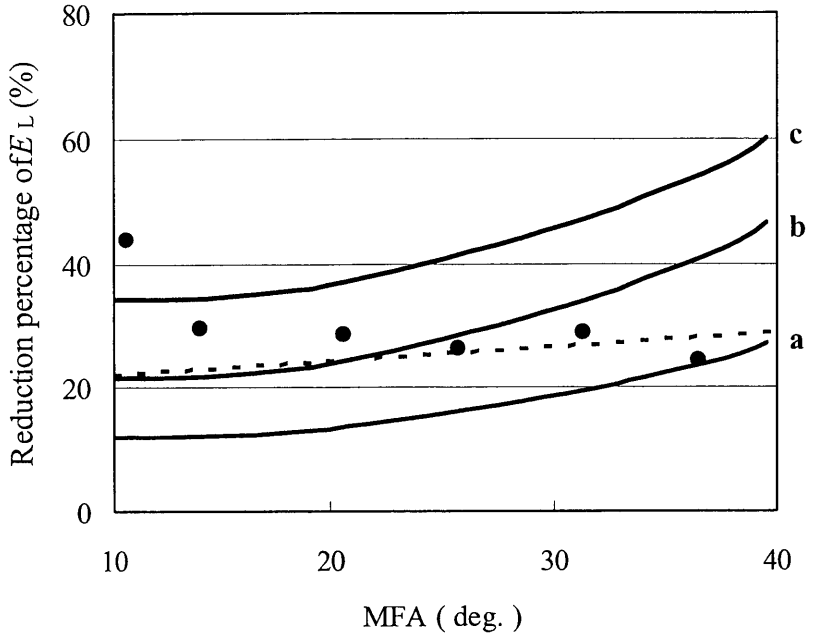

Fig.3-4. The relationship between the percentage reduction of the longitudinal Young's modulus (E_L) and the MFA—simulations based on two hypotheses.

Conditions for the simulation:

1) The weight ratio of the rigid crystal to whole substance in each layer of the secondary wall is assumed to be 10% (S2) and 5% (S1).
2) The oven-dried density is assumed to be 0.22g/cm^3.
3) The solid line shows the case in which E_{matr} increases monotonously from 2GPa at the FSP to **a**; 4GPa, **b**; 7GPa, **c**; 10GPa at the oven-dried state, and there is no unstable domain in the CMF.
4) The broken line shows the case in which E_{matr} increases monotonously from 2GPa at the FSP to 4GPa at the oven-dried state, and there is an unstable domain in the CMF. The weight ratio of the unstable domain to whole substance in each layer of the secondary wall is 4.5% (S2) and 2.25% (S1).

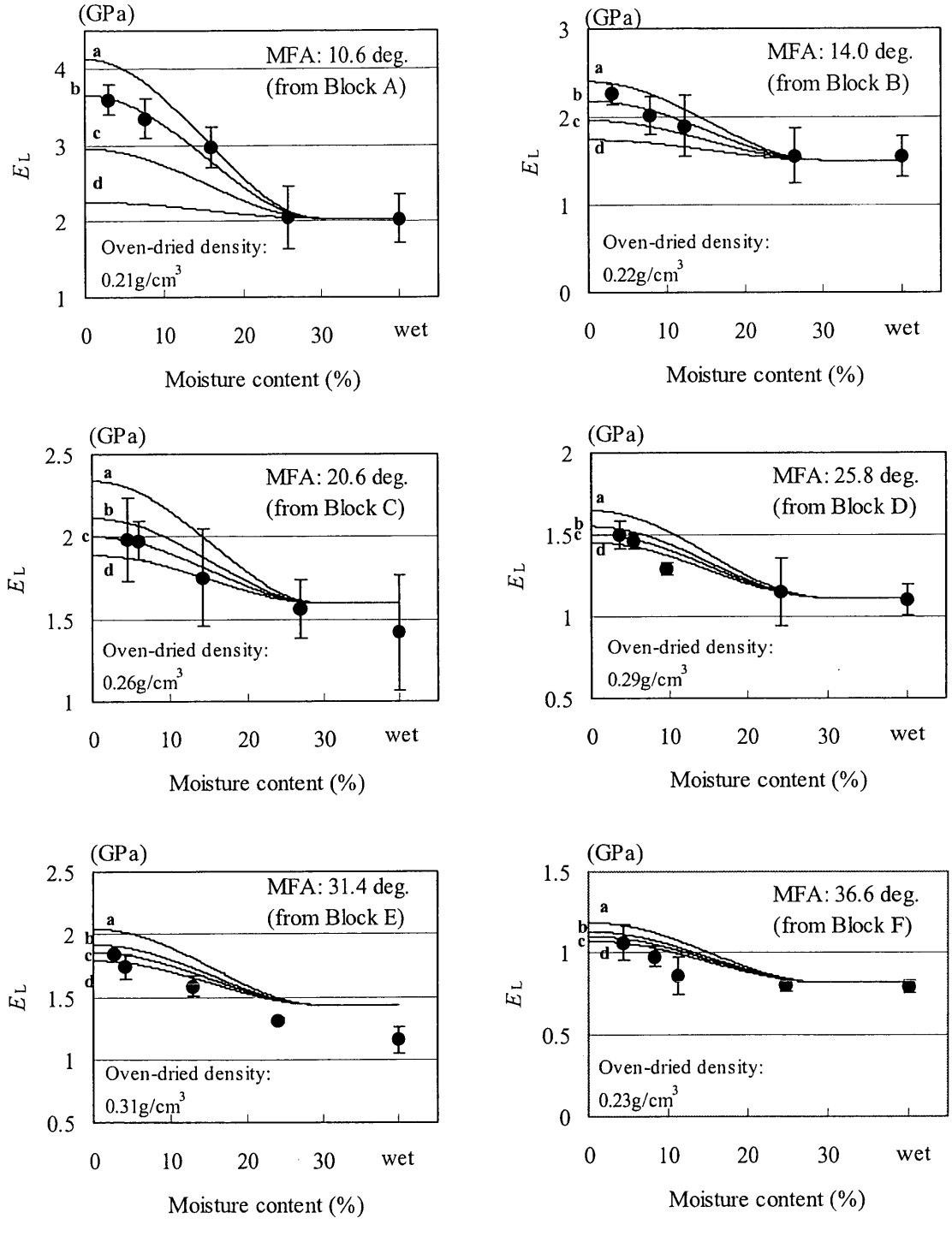

Figs.3-5. The Moisture content dependencies of the longitudinal Young's modulus of the wood (E_L)—simulation using a wood fiber model.

Conditions of the simulation:

1) The CMF contains an unstable domain that changes between the quasi-crystal and

the quasi-amorphous states in accordance with moisture adsorption.

2) E_{matr} increases monotonously from 2GPa at the FSP to 4GPa at the oven-dried state in accordance with moisture desorption.
3) The weight ratios of the rigid crystal and the unstable domain to whole substance in each layer of the secondary wall are assumed in Table 3-2.

Experiment:

1) The experimental results were obtained from a specimen of sugi wood.
2) Each plot represents an average value, and the error bar stands for the standard deviation.

Table 3-2. Simulation conditions in Fig.3-5---weight ratios of the rigid crystal and the unstable domains to whole substance in each layer of the secondary wall.

(a) The weight ratio of the rigid crystal to whole substance in each layer of the secondary wall.

(b) The weight ratio of the unstable domain to whole substance in each layer of the secondary wall.

(a)

Specimen	A	B	C	D	E	F
MFA (deg.)	10.6	14.0	20.6	25.8	31.4	36.6
density (g/cm^3)	0.21	0.22	0.26	0.29	0.31	0.22

(b)

specimen	condition **a**	condition **b**	condition **c**	condition **d**
A	14% (S2), 7% (S1)	10% (S2), 5% (S1)	5% (S2), 2.5% (S1)	0% (S2), 0% (S1)
B	10% (S2), 5% (S1)	6% (S2), 3% (S1)	3% (S2), 1.5% (S1)	0% (S2), 0% (S1)
C	9% (S2), 4.5% (S1)	6% (S2), 3% (S1)	3% (S2), 1.5% (S1)	0% (S2), 0% (S1)
D	6% (S2), 3% (S1)	4% (S2), 2% (S1)	2% (S2), 1% (S1)	0% (S2), 0% (S1)
E	10% (S2), 5% (S1)	6% (S2), 3% (S1)	3% (S2), 1.5% (S1)	0% (S2), 0% (S1)
F	12% (S2), 6% (S1)	8% (S2), 4% (S1)	4% (S2), 2% (S1)	0% (S2), 0% (S1)

CHAPTER 4 THE RELATIONSHIP BETWEEN THE LONGITUDINAL TENSILE CREEP BEHAVIOR AND THE FINE STRCTURE OF THE WOOD CELL WALL

4.1 Introduction

To clarify the mechanical properties of wood, it is very important to investigate the behavior of wood subjected to the longitudinal simple tensile load. By understanding those behaviors, the author can discuss the mechanical properties of wood from the viewpoint of the fine structure of the cell wall. As the one of those studies, the author focused his attention on the relationship between the longitudinal Young's modulus and the moisture content in the previous Chapters 2 and 3. As a result, the author obtained the new image of the behavior of wood CMF in relation to the moisture dependent properties of the Young's modulus of the wood. Then, to understand the longitudinal mechanical properties of wood deeply, the author needs to investigate the longitudinal viscoelastic properties of wood. The studies on the viscoelastic properties of wood began on a large scale in the 1960s, which includes the mechano-sorptive creep (Armstrong 1972, Armstrong and Kingston 1960, Armstrong and Christensen 1961, Yamada et al. 1961). Subsequently, there have been many reports on the viscoelastic properties of wood (Grossman 1976, Takemura 1967, 1968, 1970a, 1970b, 1972a and 1972b, Mukudai and Yata 1986, 1987 and 1988, Navi et al.2002). Most of those reports involved bending or compression tests using wood beams since the results using wood beams are practically important for building or furniture engineering. On the other hand, there are few reports on the longitudinal tensile tests except a few example (e.g. Navi et al.2002). This is because the structural member for building is usually subjected not to tensile force but to bending or compressive load, furthermore, the viscoelastic measurements required for the longitudinal tensile tests take a very long time to perform, and it is difficult to detect a small amount of deformation caused by the longitudinal tensile load.

To understand and explain the origin of the viscoelastic properties of the wood, it is required to clarify the viscoelastic properties of wood from the viewpoint of the fine structures and properties of the constituent materials in the wood cell wall. It is

considered that the mechanical properties determined from the longitudinal tensile test using a homogeneous clear specimen would reflect the fine structure of the cell wall (Navi et al.2002, Yamamoto and Kojima 2002, Kojima and Yamamoto in press). Therefore, it is necessary to measure the longitudinal viscoelastic properties of wood using a thin specimen which is approximately regarded as a single fiber. Among the fine structure of the wood cell wall, the microfibril angle (MFA) of the middle layer of the secondary wall (S2) likely plays a very important role in controlling various mechanical properties of wood and the wood cell wall e.g. the longitudinal Young's modulus (Cave 1968, Sobue and Asano 1976, Page et al.1977, Norimoto et al.1981, Yamamoto and Kojima 2002), and, the anisotropic swelling and shrinkage (Barber and Meylan 1964, Meylan 1972, Cave 1972b, Yamamoto 1999, Yamamoto et al.2001). It is easily expected that the MFA gives a certain influence on the viscoelastic properties of wood, moreover, it is also expected that the viscoelastic properties of wood are affected by the moisture content. However, no positive verification has been obtained yet.

In this chapter, the author focused the longitudinal tensile creep behavior of wood, especially in relation to the MFA and the moisture content, using a sugi (*Cryptomeria japonica* D.Don) early-wood thin specimen. Moreover, the author tried to clarify the roles of the wood cell wall constituent materials on the longitudinal tensile viscoelastic properties.

4.2 Material and methods

4.2.1 Material

A 40-year-old, 20-cm DBH sugi (*Cryptomeria japonica* D.Don) growing in Nagoya University experimental forest was studied. Blocks were cut from the sapwood of the vertical stem. Some blocks were cut from the juvenile wood. After cutting the blocks, they were boiled in hot water for 10minutes to saturate them. Then, homogeneous tangential sections (70×8×0.2mm in L×T×R directions) were prepared from the early-wood region of each block using a sliding microtome, and were used for the tensile test. Early-wood specimen used to measure the oven-dried density was cut from the same annual rings as the specimen used for the creep test.

4.2.2 Methods

(a) Determining the creep strain

In general, the strain gauge method is used to detect the strain of deformation induced by the tensile test. Then, the applicability of the strain gauge method was discussed. The effect of the thickness of the early-wood specimen prepared from the sapwood region (70×8×0.2~0.8mm in L×T×R directions) on the apparent longitudinal Young's modulus was measured using the strain gauge method with wet specimen. The mean value of the MFA of the specimen was 15.5° (the standard deviation 1.22, specimen number 4). The result is shown in Fig.4-1. In this figure, the apparent Young's modulus is larger in specimen 0.2~0.5mm thick than in those over 0.6mm thick. This suggests that the effects of the rigidity of the strain gauge and the quick-drying glue become manifest in specimen less than 0.5mm thick. That is, specimen must be at least 0.6mm thick to eliminate the effect of the rigidity of the strain gauge and glue when the strain gauge method is used to detect the mechanical strain. In this study, homogeneous flat-sawn specimen of early-wood was used for the creep test. Since the specimen ware often less than 0.5mm thick, it is improper to adopt the strain gauge method to detect the creep strain. Therefore, to detect the creep strain, the author measured the distance between two dots marked on the grain using a traveling microscope with an xy-microstage directly.

(b) Determining the creep load

The shape of the stress-strain curve was investigated to determine the proportional limit. The proportional limit was 12~15MPa (average 14.0MPa) regardless of the thickness of the specimen, as shown in Fig.4-2. Therefore, a load of 14.2 MPa, corresponding to the proportional limit of the normal early-wood specimen was used for the creep load.

(c) The longitudinal creep test

To prevent slippage at the clamps during the creep test, pieces of sandpaper were attached to each edge of the specimen using quick-drying glue. Then, the specimen was put in a small air-conditioned cabinet. In this study, moisture contents of specimen were controlled at oven-dry (MC2%), air-dry (MC15%) and the fiber saturation point (FSP) (MC25%) at 20°C. The moisture content were controlled using H_2O, NaCl aq., P_2O_5 powder, at 100%, 76%, 0%RH at 20°C, respectively. The creep test was performed in an airtight chamber, in which the air was circulated by a micro-electric fan, and the RH was controlled with above three materials at 20°C. After the specimen was conditioned in the cabinet for a few days, it was attached to a hand-made tensile testing machine in the chamber. Two spots 20~30mm apart along the grain were marked with black paint to measure the displacement caused by the tensile load. To measure the distance between the two dots, a traveling microscope with an xy-microstage (0.001mm accuracy) was used. A load of 14.2MPa, corresponding to the proportional limit of sugi early-wood, was applied to the specimen as a dead load. The initial displacement was measured soon after applying the load and was considered an instantaneous displacement. Then, the displacement was detected every few hours for several hundred hours. After the creep test was finished, a time-creep compliance curve was obtained. The creep tests were performed for a broad range of MFA.

(d) Microfibril angle determination

After the creep test was performed, the microfibril angle (MFA) in the S2 layer of each specimen was measured using an X-ray diffractometer (Shimadz, XD-D1w type) (Yamamoto et al. 1993).

(e) Wood density measurement

Wood density was determined by the gravimetrical method using mercury impregnation. The wood density of each specimen was determined after small specimen prepared reaching constant weight in an oven at 105°C for 24 hours. To measure oven-dried volume, the mercury displacement technique was employed.

(f) Simulation using the simplified viscoelastic model

A simplified model explaining the longitudinal creep properties is shown in Fig.4-3. The model consists of an independent spring (spring1) and a Voigt element (spring2 and dashpot2) in series. The elastic modulus of spring1, spring2 and the viscosity coefficient of dashpot2 are denoted by E_1, E_2, η_2, respectively. Using this creep model, the following equations are derived:

$$\varepsilon(t) = \sigma\left\{\frac{1}{E_1} + \frac{1}{E_2}(1 - e^{-t/\lambda_2})\right\} \quad , \quad \lambda_2 = \frac{\eta_2}{E_2} \qquad \text{(Eqs.4-1)}$$

$$J(t) = \frac{1}{E_1} + \frac{1}{E_2}(1 - e^{-t/\lambda_2}) \quad , \quad \lambda_2 = \frac{\eta_2}{E_2} \qquad \text{(Eqs.4-2)}$$

where $\varepsilon(t)$, $J(t)$, σ, t and λ_2 denote the creep strain, creep compliance, loaded stress, time, and the retardation time, respectively.

Then, the parameters E_1, E_2,and η_2 are transformed as follows:

$$E_1 \longrightarrow E_1^W \left(= \frac{\rho^W}{\rho_0} E_1\right),$$

$$E_2 \longrightarrow E_2^W \left(= \frac{\rho^W}{\rho_0} E_2\right),$$

$$\eta_2 \longrightarrow \eta_2^W \left(= \frac{\rho^W}{\rho_0} \eta_2\right)$$

where ρ^W, ρ_0, E_1^W, E_2^W and η_2^W stand for the density of the cell wall, that of oven-dried wood, the substantial elastic modulus of spring1 and spring2, the substantial viscosity coefficient of dashpot2, respectively. The author can rewrite Eqs.4-2 as the follow:

$$J^W(t) = \frac{1}{E_1^W} + \frac{1}{E_2^W}(1 - e^{-t/\lambda_2^W}) \qquad \lambda_2^W = \lambda_2 = \frac{\eta_2}{E_2} \qquad \text{(Eqs.4-3)}$$

It is quite natural to consider $J^W(t)$ as the substantial creep compliance of the cell wall in

the longitudinal direction. The author tried to determine the values of the unknown parameters (E_1^W, E_2^W, η_2^W, λ_2^W) to simulate the experimental results quantitatively. Finally, the author discusses the physical meanings of those estimated values, and their dependencies on the MFA.

4.3 Results and discussion

4.3.1 The longitudinal tensile creep properties

It is well known that the mechanical properties of wood are affected by the density. Viscoelastic property is also affected by the density. To understand the viscoelastic behavior of wood as a cell wall property, it is necessary to transform $J(t)$ into a substantial value by considering the effect of the density of the specimen. To transform the longitudinal Young's modulus of wood, E_L, into the substantial Young's modulus of the wood cell wall, E_L^W, the author can use the following formula:

$$E_L^W = E_L \cdot \frac{\rho^W}{\rho_0}$$

where, ρ^W is the density of the cell wall, and ρ_0 is that of oven-dried wood. For linear viscoelastic materials, the substantial creep compliance of the cell wall in the longitudinal direction, $J^W(t)$, is calculated as follows:

$$J^W(t) = J(t) \cdot \frac{\rho_0}{\rho^W}$$

Figures4-4 show the time dependencies of the substantial creep compliance of the cell wall $J^W(t)$ in relation to the MFA. Three curves in each figure show the results conducted at three moisture conditions (●: oven-dry, ○: air-dry, ▲: FSP). As seen from these figures, the instantaneous compliance appeared immediately after the load was applied. Subsequently, the total creep compliance increased with time and peaked after several hundred hours. These observations concur with various experimental reports on the bending creep properties under a steady-moisture condition using the wood beams (Hearmon and Paton 1964, Armstrong 1972). Since the instantaneous compliance (=the instantaneous deformation) highly depends on the MFA and moisture content, it is difficult to discuss the MFA and the moisture content on the creep behavior by using the results displayed in Figs.4-4. Then, the author needs to calculate the substantial creep function of the cell wall, $\varphi^W(t)$, which is calculated by subtracting the initial instantaneous compliance from $J^W(t)$. Figures4-5 show the substantial creep function of the cell wall, $\varphi^W(t)$.

At first, the relationship between the moisture content and the longitudinal tensile

creep behavior was discussed. It is clear that the amount of variations of the creep function is affected by the moisture content from Figs4-5. In the low moisture content region (oven-dry state), the variation of the creep function was smaller than in other moisture content states. As the moisture content become higher, the variation of the creep function also becomes larger. That is to say that the longitudinal tensile creep behavior clearly shows the dependency of the moisture content. Furthermore, the dependency of the moisture content is remarkable in the large MFA region, however, in the smallest MFA region (MFA:12.0deg.), the dependency of the moisture content is not clear. This is because that the longitudinal tensile creep behavior highly reflected the properties of the wood cell wall constituents. Since the longitudinal tensile creep behavior for a small MFA was affected by the CMF, which may be less affinitive to the moisture, the variations of the creep function were very small even if the moisture content changed. On the other hand, for the large MFA, since the matrix substance in the cell wall, which may be highly affinitive to the moisture, affected the longitudinal tensile creep behavior, the variations of the creep function were more distinctive when the moisture content changed.

Next, the relationship between the MFA and the longitudinal tensile creep behavior was discussed. Figures4-6 show the relationship between the MFA and the substantial creep function of the cell wall. In Figs.4-6, it is clear that the variation of the creep function was very small in the small MFA region, and as MFA increased, the variation became larger. This shows that the longitudinal tensile creep properties of wood are highly dependent on the MFA. This is because the viscoelastic behavior to the longitudinal tensile load directly reflects the properties of the cell wall constituents and their arrangement in the cell wall. In the region of small MFA, because the longitudinal creep deformation was affected by the CMF, which is much more viscous than the matrix substance in the cell wall constituents, the variation of the creep function becomes very small. By contrast, at a large MFA, the matrix substance in the cell wall affects the longitudinal tensile creep behavior, since the mechanical contribution of the CMF decreases. Since the matrix substance is less viscous than the CMF, the creep function becomes several times larger than at a small MFA.

4.3.2 Simulated results using the simplified viscoelastic model

The observed $J^W(t)$ was simulated using the simplified viscoelastic model formulated as Eqs.4-3. It is quite natural to consider that the values of the parameters in the simulation reflect intrinsic information on the fine structure and internal properties of the cell wall constituents. Figures4-7 show the dependency of the fitted values of the E_1^W, E_2^W, η_2^W and λ_2^W on the MFA. As seen in Figs.4-7, the value of E_1^W decreased concavely as the MFA increased, which concurs with the previous results reported by Cave (1968), Sobue and Asano (1976), Page et al. (1977) and Norimoto et al. (1981). The MFA dependencies of the simulated values of E_2^W and η_2^W were steeper than that of E_1^W, as shown in Figs.4-7. The values of E_2^W and η_2^W tended to be small in the MFA region larger than 20deg., and become very large in the region of smaller MFA. The values of E_2^W and η_2^W become larger as the moisture content becomes smaller in the region of MFA larger than 20deg., however, the values at the oven-dried state become smaller than the other two moisture states. This reason was not clear from this simplified viscoelastic model. The value of E_2^W is an indicator of the smallness of the creep deformation. The value of E_2^W in the region of small MFA is much larger than that at large MFA region. In the region of small MFA, this is why the longitudinal creep deformation was affected by the CMF, which is much more viscous than the matrix substance in the cell wall constituents. Conversely, in the region of large MFA, the longitudinal creep deformation is affected by the matrix substance, which is much less viscous than the CMF. The values of η_2^W and λ_2^W are indicators of the smallness of the creep rate. The value of η_2^W is clearly dependent on the MFA. In the small MFA region, the value of η_2^W is much larger than that in the large MFA region, since the creep rate is affected mainly by the CMF. Conversely, the value of η_2^W decreases as MFA increases, since the longitudinal creep rate is markedly affected by the matrix substance in the region of large MFA. The value of λ_2^W is not dependent on the MFA clearly. This can be explained as follows. The value of λ_2^W is calculated as the ratio of η_2^W and E_2^W. The MFA dependency of η_2^W was more or less similar as that of E_2^W. Therefore, the value of λ_2^W becomes more or less constant regardless of the MFA.

The author estimated the unknown parameters of the simplified model by comparing the simulation with the experimental results. The parameters are highly

dependent on the MFA. This is because the tensile creep deformation is affected by the arrangement of the cell wall constituents, namely the CMF framework and matrix substance. To clarify the effect of the cell wall constituents on the longitudinal tensile creep property of wood, the author must construct a multi-layered cell wall model considering the composite and fine structures of the cell wall lamella.

4.4 Conclusion

In this chapter, the author examined the dependency of the longitudinal tensile creep behavior of thin clear wood specimen of sugi on the MFA and the moisture content. As a result, the following conclusions were made:

The longitudinal tensile creep behavior is highly dependent on both the moisture content and the MFA. In the large MFA region, there is large difference in the variation of the creep function among three moisture content states, the oven-dried, the air-dried, and the fiber saturation point. On the other hand, in the small MFA region, there is very little difference in the creep function among three moisture content states since the creep deformation in the small MFA region is affected by the CMF, which is very viscous and less reactive to the moisture. Conversely, in the large MFA region, the creep deformation is affected by the matrix substance, which is much less viscous than the CMF and very reactive to the moisture.

These are the reason that the longitudinal tensile creep behavior as well as the other mechanical properties was affected by the behavior of the cell wall constituents directly. To clarify the effect of the cell wall constituents on the longitudinal tensile creep property in detail, the author needs to construct a multi-layered cell wall model that considers the composite and fine structures of the cell wall lamella.

4.5 Summary

To measure the mechanical properties of the wood as the behavior of the cell wall, it is required to perform the longitudinal tensile test using a thin clear wood specimen which is approximately regarded as a single wood fiber. In this chapter, the author tried to understand the tensile creep behavior of wood from the viewpoint of the fine structure and properties of the constituent materials in the wood cell wall.

Microtomed thin specimen of early-wood of sugi (*Cryptomeria japonica* D.Don) was used for the longitudinal tensile creep test. The creep test was conducted three moisture content states (oven-dry, air-dry, fiber saturation point (FSP)) with a broad range of the microfibril angle (MFA).

Following results were obtained. The longitudinal tensile creep behavior was highly dependent on both the moisture content and the MFA. In the small MFA region, the creep function was very small. In the large MFA region, the creep function was very large. In the low moisture content region, the creep function was very small, and in the high moisture content region, it became very large. These were the reason that the longitudinal tensile creep behavior was directly affected by the fine structure and internal properties of the cell wall constituents, namely, the CMF and the matrix substance.

Figures in Chapter 4

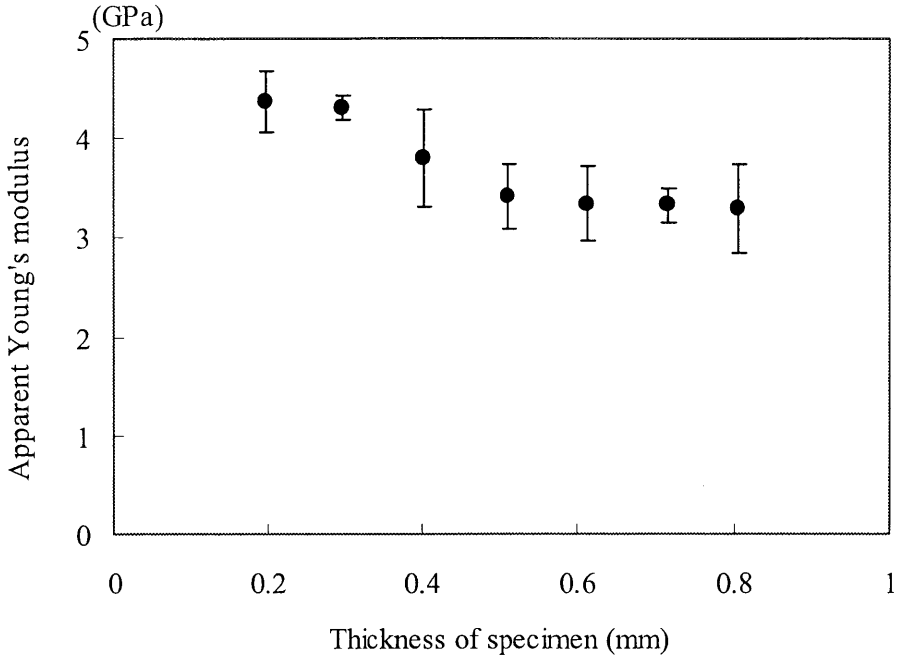

Fig.4-1. The relationship between the thickness of the sugi early-wood specimen and the apparent longitudinal Young's modulus measured using the strain gauge method.

Notes:

1) Each plot represents average values
2) The error bar shows the standard deviation.
3) All the tests were conducted under wet condition.

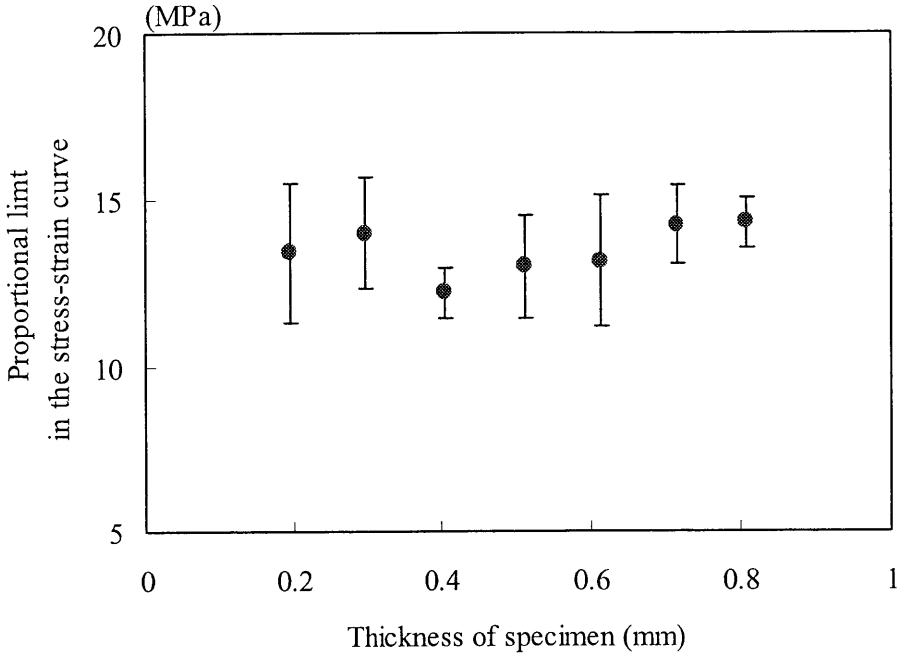

Fig.4-2. The relationship between the thickness of the sugi early-wood specimen and the proportional limit in the stress-strain curve.

Notes:

1) Each plot represents average values
2) The error bar shows the standard deviation.
3) All the tests were conducted under wet condition.

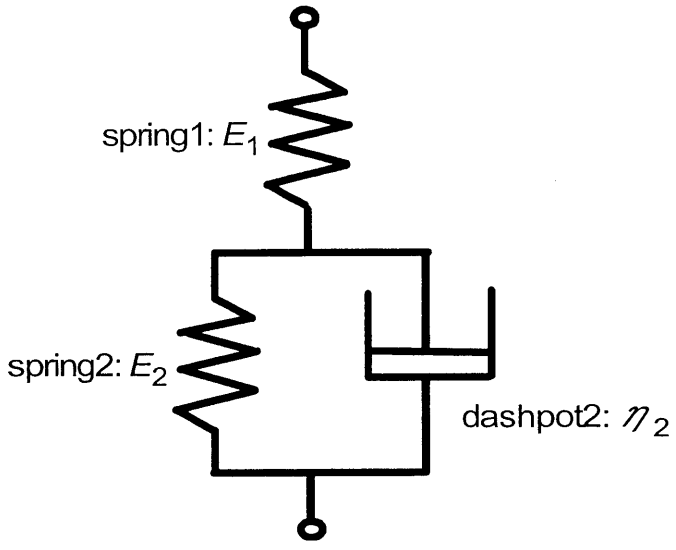

Fig.4-3. A simplified viscoelastic model of wood for simulating the longitudinal creep behavior.

Note:

Spring1 and spring2 have elastic modulus E_1 and E_2, respectively, and dashpot2 has viscosity coefficient η_2.

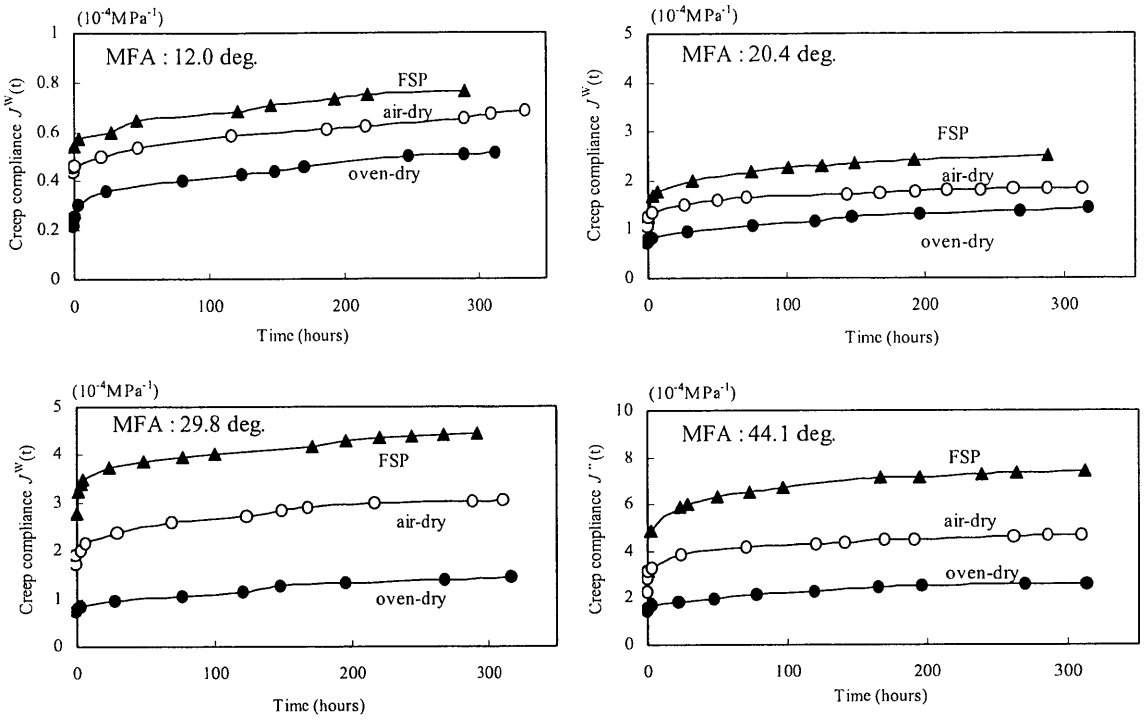

Figs.4-4. The moisture dependencies of the substantial creep compliance of the cell wall in the longitudinal direction $J^W(t)$.

Legends: ●; oven-dry, ○; air-dry, ▲; FSP

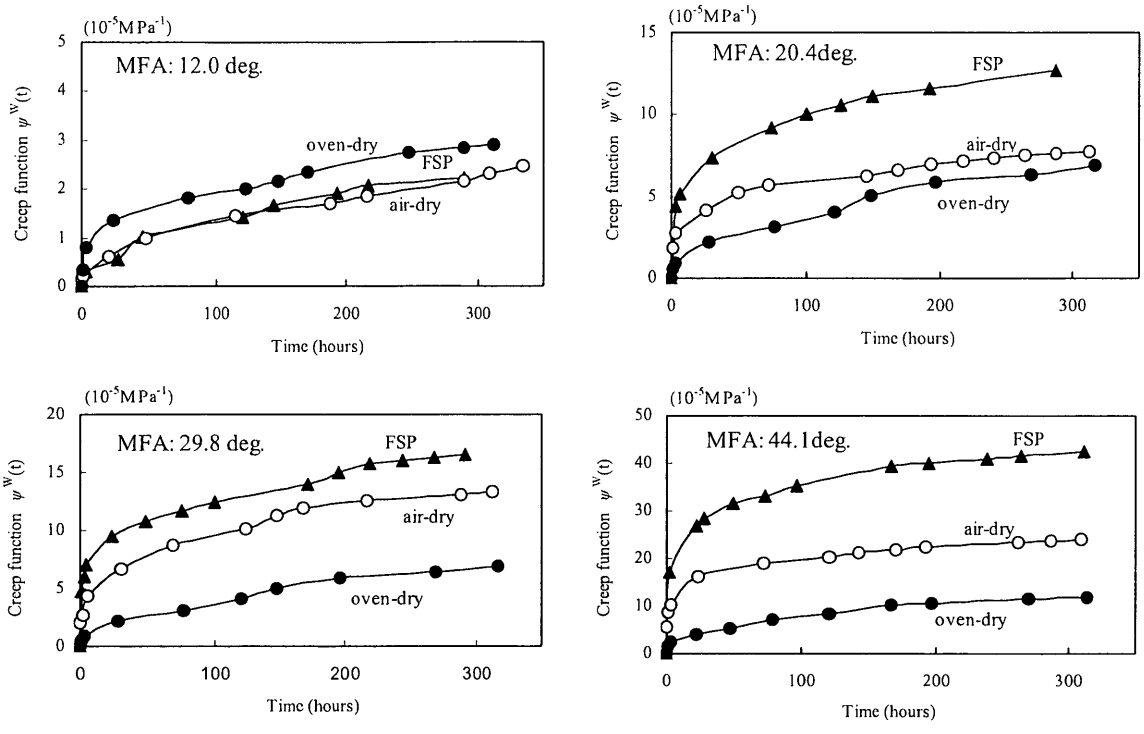

Figs.4-5. The moisture dependencies of the substantial creep function of the cell wall in the longitudinal direction $\varphi^{W}(t)$.

Legends: ●; oven-dry, ○; air-dry, ▲; FSP

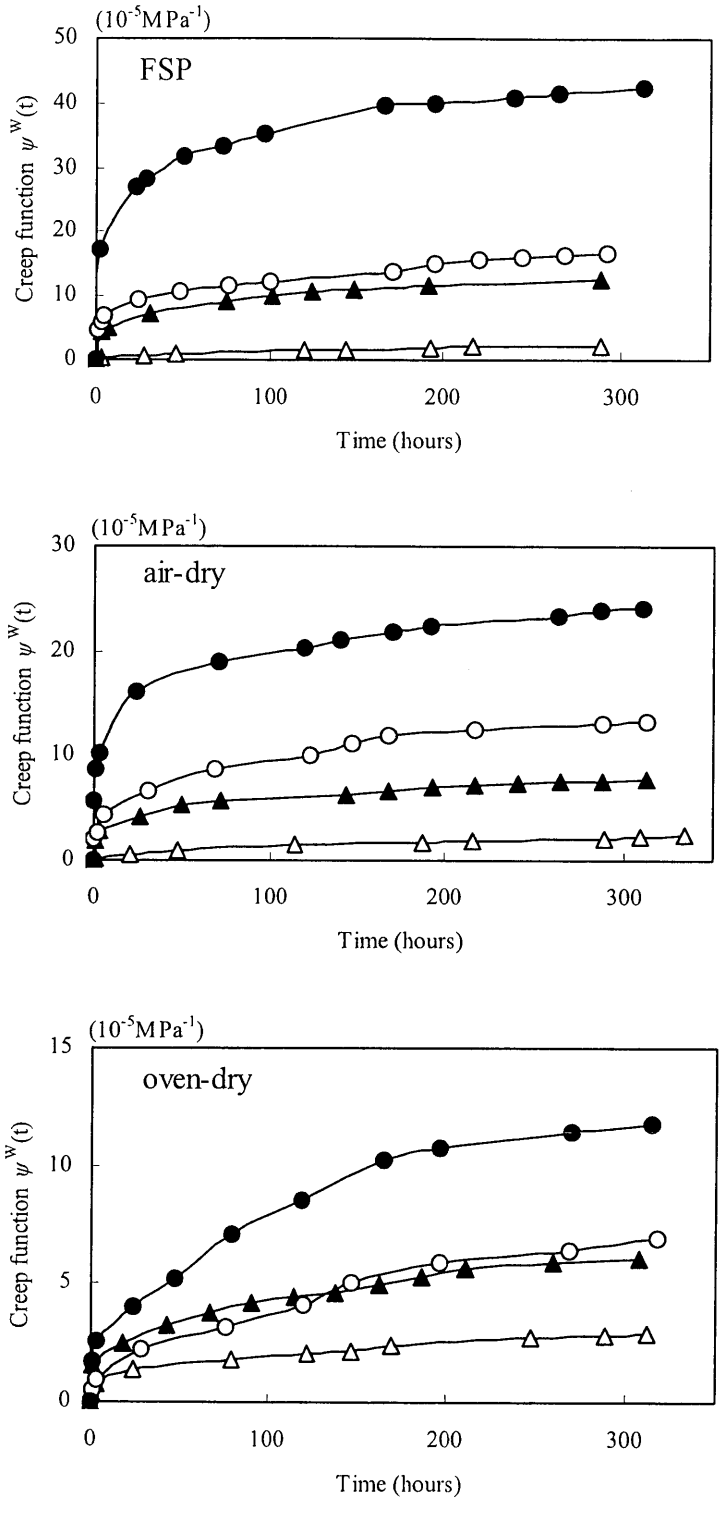

Figs.4-6. The MFA dependencies of the substantial creep function of the cell wall in the longitudinal direction $\varphi^{W}(t)$.

Legends: Δ; MFA12.0deg., ▲; MFA20.4deg., ○; MFA29.8deg., ●; MFA44.1deg.

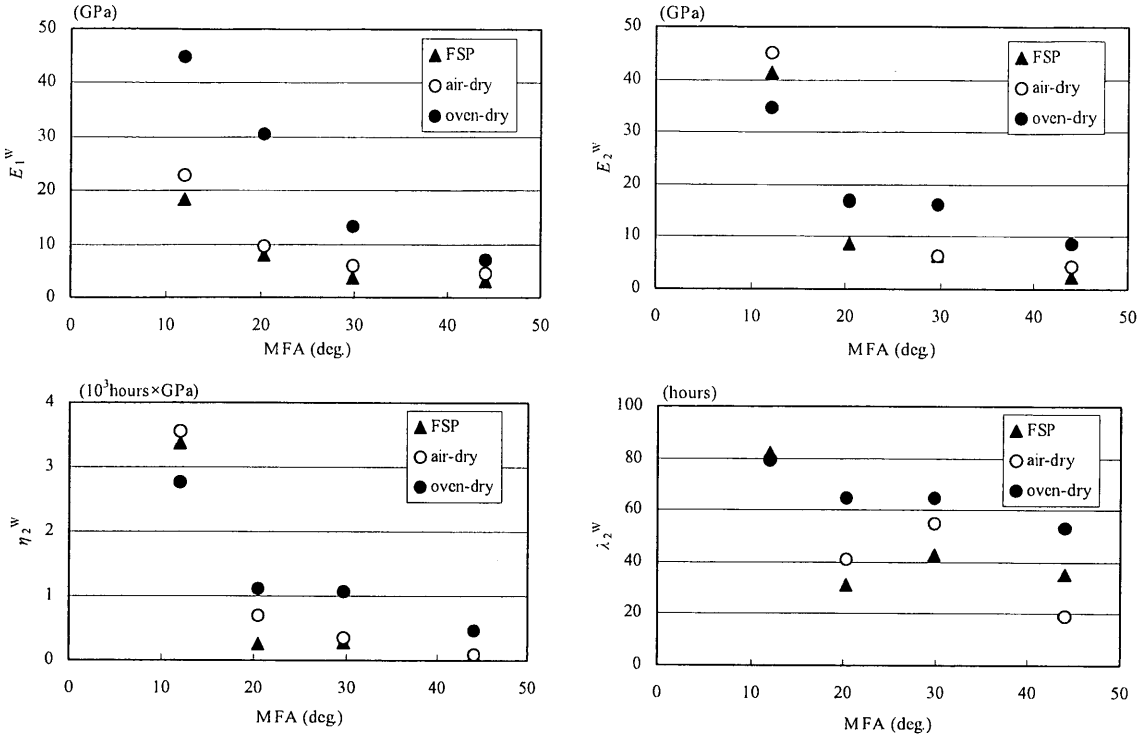

Figs.4-7. The MFA dependencies of calculated values of the parameters in the simplified model.

Legends: ●; oven-dry, ○; air-dry, ▲; FSP

GENERAL DISCUSSION AND CONCLUSION

The aim of this study is to clarify the mechanical properties of wood in relation to the fine structure of wood cell wall.

In Chapter 2, the author tried to formulate the longitudinal Young's modulus of the isolated wood fiber on the basis of the reinforced-matrix hypothesis. Some case studies on the elastic behaviors of the wood were given using the newly-derived model. Then, the author estimated the fine structure and internal properties of the cell wall constituents peculiar to wood by examining the values of the parameters which are optimized through the reasonable simulation. As the inevitable consequence, some hypotheses (possibilities) on the microscopic properties of the cell wall constituents were predicted.

In Chapter 3, the author measured the longitudinal Young's modulus of a clear wood specimen having various MFA in relation to the moisture content. The proprieties of the hypotheses (possibilities) proposed in Chapter 2 were examined on the basis of both the experiment and the simulation. The experiment revealed that the longitudinal Young's modulus tended to decrease as the moisture content increased below the FSP, and it became constant above the FSP. Moreover, the reduction of the longitudinal Young's modulus due to water sorption tends to increase more remarkable in specimen with a small MFA than in those with a large MFA, or to be almost constant regardless of the MFA. The simulation using a wood fiber model well supported the hypothesis that there is an intermediate domain between rigid crystal and completely disordered amorphous domains in the wood CMF bundle, and such a domain fluctuates between quasi-crystal and quasi-amorphous states in accordance with the moisture adsorption. Then, based on above hypothesis, the author proposed the new image of the CMF structure in the wood cell wall visually.

In above Chapters, the author thought wood as the elastic body, however, it is very important to clarify the viscoelastic properties of wood in order to use forest products as structural member for buildings or furniture. There are few reports on the longitudinal tensile viscoelastic tests, which reflects the properties of the cell wall more directly. Moreover, the relationship between the viscoelastic properties and the fine structure of

wood cell wall has not been solved. To understand and explain the origin of the viscoelastic properties of wood, it is necessary to comprehend it from the viewpoint of the fine structures and properties of the constituent materials in the wood cell wall. In Chapter 4, the author studied the dependency of the longitudinal tensile creep behavior of thin clear wood specimen on the MFA and the moisture content. Moreover, the author analyzed the experimental results by using a simplified viscoelastic model, and evaluated the values of parameters in the model. The longitudinal tensile creep behavior is highly dependent on both the moisture content and the MFA. That is to say that the creep deformation is larger as the MFA becomes larger, as the moisture content becomes larger. These were the reason that the longitudinal tensile creep behavior was directly affected by the fine structure and internal properties of the cell wall constituents, namely, the CMF and the matrix substance.

In this paper, the author focused the physical properties of wood in the longitudinal direction in relation to the fine structure of cell wall. Based on the methods and the results proposed in this thesis, the author hopes to construct a model which can explain many properties of wood, and to clarify the fine structure of the CMF, the matrix substance, and their interface structure.

REFERENCES

Aoki T, Yamada T. (1977) Creep of wood during decrystallization and of decrystallized wood (in Japanese). 23: 10-16.

Arima T. (1967) The influence of high temperature on compressive creep of wood (in Japanese). Mokuzai Gakkaishi. 13: 36-40.

Armstrong L D. (1972) Deformation of wood in compression during moisture movement. Wood Science. 5: 81-86.

Armstrong L D, Kingston R S T. (1960) Effect of moisture changes on creep in wood. Nature. 185: 862-863.

Armstrong L D, Christensen G N. (1961) Influence of moisture changes on deformation of wood under stress. Nature. 191: 868-869.

Barber N F, Meylan B A. (1964) The anisotropic shrinkage of wood. A theoretical model. Holzforschung. 18: 146-156.

Barber N F. (1968) A theoretical model of shrinking wood. Holzforschung. 22: 97-103.

Barrett J D, Schniewind A P, Taylor R L. (1972) Theoretical shrinkage model for wood cell walls. Wood Science. 4: 178-192.

Cave I D. (1968) Anisotropic elasticity of the plant cell wall. Wood Science and Technology. 2: 268-298.

Cave I D. (1972a) Swelling of a fibre reinforced composite in which the matrix is water reactive. Wood Science and Technology. 6: 157-161.

Cave I D. (1972b) A theory of shrinkage of wood. Wood Science and Technology. 6: 284-292.

Cave I D. (1978a) Modelling moisture-related mechanical properties of wood. PartI: Properties of the wood constituents. Wood Science and Technology. 12: 75-86.

Cave I D. (1978b) Modelling moisture-related mechanical properties of wood. PartII: Computation of properties of a model of wood and comparison with experimental data. Wood Science and Technology. 12: 127-139.

Cousins W J. (1976) Elastic modulus of lignin as related to moisture content. Wood Science and Technology. 10: 9-17.

Cousins W J. (1978) Young's modulus of hemicellulose as related to moisture content.

Wood Science and Technology. 12: 161-167.

Furuta Y, Notimoto M, Yano H. (1998) Thermal-softening properties of water swollen wood. V. The effect of drying and heating histories. Mokuzai Gakkishi. 44: 82-88.

Fusitani M. (1968a) Effect of delignifying treatment on static viscoelasticity of wood. I. Stress relaxation (in japanese). Mokuzai Gakkaishi. 14: 11-17.

Fusitani M. (1968b) Effect of delignifying treatment on static viscoelasticity of wood. II. Temperature dependence of stress relaxation in the water-saturated condition (in japanese). Mokuzai Gakkaishi. 14: 18-23.

Fusitani M. (1968c) Effect of delignifying treatment on static viscoelasticity of wood. III. Temperature dependence of stress relaxation in the absolutely dried condition (in japanese). Mokuzai Gakkaishi. 14: 160-165.

Fusitani M. (1968d) Effect of delignifying treatment on static viscoelasticity of wood. IV. Strain dependence of stress relaxation and stress dependence of creep (in japanese). Mokuzai Gakkaishi. 14: 166-171..

Grossman P U A. (1976) Requirements for a model that exhibits mechano-sorptive behaviour. Wood Science and Technology. 10: 163-168.

Hearmon R F S, Paton J M. (1964) Moisture content changes and creep of wood. Forest Product Journal. 14: 357-359.

Ishikawa A, Okano T, Sugiyama J. (1997) Fine structure and tensile properties of ramie fibres in the crystalline form of cellulose I, II, III_I and IV_I. Polymer. 38 (2) 463-468.

Ishikawa A, Kuga S, Okano T. (1998) Determination of parameters in the mechanical model for cellulose III fiber. Polymer. 39: 1875-1878.

Kerr A J, Goring D A I. (1975) The ultrastructural arrangement of the wood cell wall. Cellulose Chemical and Technology. 9: 563-573.

Kitahara K, Yukawa K. (1964) The influence of the change of temperature on creep in bending (in Japanese). Mokuzai Gakkaishi. 10: 169-175.

Kojima Y, Yamamoto H. (in press) Properties of cell wall constituents in relation to longitudinal elasticity of wood. Part 2.Origin of the moisture dependency of the longitudinal elasticity of wood. Wood science and Technology.

Kollmann F, Krech H. (1960) Dynamic measurement of damping capacity and elastic properties of wood. Holz als Roh-und Werkstoff. 18: 41-54.

Koponen S, Toratti T, Kanerva P. (1989) Modelling longitudinal elastic and shrinkage properties of wood. Wood Science and Technology. 23: 55-63.

Koponen S, Toratti T, Kanerva P. (1991) Modelling elastic and shrinkage properties of wood based on cell structure. Wood Science and Technology. 25: 25-32.

Mallick P K. (1988) Fiber-reinforced composites. Materials, manufacturings, and design. pp.73-128. New York: Marcell Deckker Inc.

Mark R E. (1967) Cell wall mechanics of tracheids. pp.27-58. New York: Yale University Press.

Meylan B A. (1972) The influence of microfibril angle on the longitudinal shrinkage-moisture content. Wood Science and Technology. 6: 293-301.

Moriizumi S, Okano T. (1978) Viscoelasticity and structure of wood. IV. Behavior of crystal lattice strain depended on moisture content and time (in Japanese). Mokuzai Gakkaishi. 24: 1-6.

Mukudai J, Yata S. (1986) Modeling and simulation of viscoelastic behavior (tensile strain) of wood under moisture change. Wood Science and Technology. 20: 335-348.

Mukudai J, Yata S. (1987) Further modeling and simulation of viscoelastic behavior (bending deflection) of wood under moisture change. Wood Science and Technology. 21: 49-63.

Mukudai J, Yata S. (1988) Verification of Mukudai's mechano-sorptive model. Wood Science and Technology. 22: 43-58.

Navi P, Pittet V, Plummer C J G. (2002) Transient moisture effects on wood creep. Wood Science and technology. 36: 447-462.

Nishino T, Takano K, Nakamae K. (1995) Elastic modulus of the crystalline regions of cellulose polymorphs. Journal of Polymer Science. Part B, Polymer Physics ED 33: 1647-1651.

Norimoto M, Ohgama T, Ono T. (1981) Young's modulus of cell wall for coniferous wood. Journal of the society of rheology. 9: 169-175.

Norimoto M, Yamada T. (1967) The effect of moisture content on modulus of rigidity and dielectric properties of wood. Wood Research. 41: 36-46.

Ozawa M, Fushitani M, Sato K, Kubo T. (1995) Bending creep behavior and acoustic

emission characteristics of wood under changing moisture conditions (in Japanese). Mokuzai Gakkaishi. 41: 978-987.

Page D H, El-Hosseiny F, Winkler K, Lancaster A P S. (1977) Elastic modulus of single wood pulp fibers. Tappi. 60: 114-117.

Saiki H. (1973) Fractography of wood. J Soc Mater Sci Japan. 22: 894-902.

Sakurada I, Nukushina A, Ito T. (1962) Experimental deformation of the elastic modulus of crystalline regions in oriented polymers. Journal of Polymer Science. 57: 651-660.

Sakurada I, Ito T, Nakamae K. (1964) Elastic moduli of polymer crystals for the chain axial direction. Macromol Chem. 75: 1-10.

Salmen L. (1982) Temperature and water induced softening behavior of wood fiber based materials. Ph.D. Thesis. (KTH, Stockholm). pp.53.

Salmen L, De Ruva A. (1985) A model for the prediction of fiber elasticity. Wood and Fiber Science. 17: 336-350.

Salmen L, Kolseth P, De Ruva A. (1985) Modelling the softening behavior of wood fibers. J Pulp Pap Sci. 11: 102-107.

Sobue N, Asano I. (1976) Studies on the fine structure and mechanical properties of wood (in Japanese). Mokuzai Gakkaishi. 22: 211-216.

Srinivasan P S. (1941) The elastic properties of molluscan shells. Quart J Indian Inst Sci. 4: 189-221.

Takemura T. (1967) Plastic properties of wood in relation to the non-equilibrium states of moisture content (continued) (in Japanese). Mokuzai Gakkaishi. 13: 77-81.

Takemura T. (1968) Plastic properties of wood in relation to the non-equilibrium states of moisture content (re-continued) (in Japanese). Mokuzai Gakkaishi. 14: 406-410.

Takemura T. (1970a) On the memory effect of wood during drying. I. The nonlinearity of the memory effect (in Japanese). Mokuzai Gakkaishi. 16: 108-114.

Takemura T. (1970b) On the memory effect of wood during drying. II. Examination of the theoretical considerations of the memory effect (nonsteady theory) by bending experiments (in Japanese). Mokuzai Gakkaishi. 16: 115-120.

Takemura T. (1972a) On the memory effect of wood during drying. III. A principle of predicting drying stresses (in Japanese). Mokuzai Gakkaishi. 18: 1-7.

Takemura T. (1972b) On the memory effect of wood during drying. IV. Prediction of drying stresses of a board (in Japanese). Mokuzai Gakkaishi. 18: 105-113.

Tokoh T, Takabe K, Fujita M, Saiki H. (1998) Cellulose synthesized by Acetobacter xylinum in the presence of acetyl glucomannan. Cellulose. 5: 249-261.

Yamada T, Takemura T, Kadita S. (1961) On the rheology of wood. III. The creep and the stress relaxation of Buna (in Japanese). Mokuzai Gakkaishi. 7: 63-67.

Yamamoto H, Okuyama T, Yoshida M. (1993) Method of determining the mean microfibril angle of wood over a wide range by the improved Cave's method (in Japanese). Mokuzai Gakkaishi. 39: 375-381.

Yamamoto H, Okuyama T, Yoshida M. (1995) Generation process of growth stresses in cell walls. VI. Analysis of the growth stress generation by using cell model having three layered (S1, S2, and I+P). Mokuzai Gakkaishi. 41: 1-8.

Yamamoto H. (1998) Generation mechanism of growth stresses in wood cell walls: roles of lignin deposition and cellulose microfibril during cell wall maturation. Wood Science and Technology. 32: 171-182.

Yamamoto H. (1999) A model of anisotropic swelling and shrinking process of wood. Part 1. Generalization of Barber's wood fiber model. Wood Science and Technology. 33: 311-325.

Yamamoto H. (in press) Role of the gelatinous layer on the origin of the physical properties of the tension wood. Journal of Wood Science.

Yamamoto H, Sassus F, Ninomiya M, Gril J. (2001) A model of anisotropic swelling and shrinking process of wood. Part 2. A simulation of shrinking wood. Wood Science and Technology. 35: 167-181.

Yamamoto H, Kojima Y. (2002) Properties of cell wall constituents in relation to longitudinal elasticity of wood. Part 1. Formulation of the longitudinal elasticity of an isolated wood fiber. Wood Science and Technology. 36: 55-74.

ACKNOWLEDGMENT

The author is deeply grateful to Professor Takashi Okuyama, Associate Professor Hiroyuki Yamamoto and Assistant Professor Masato Yoshida, Department of Forest Products, School of Agricultural Sciences, Nagoya University, for their guidance and academic counseling throughout my study.

Although I will not mention them individually, I want to thank all of the members of the Biomaterials Physics Laboratory (including who graduated during the last six years), for their assistance in various ways.

Finally, I am indebted to my mother, father, brothers and friends. Without their support, it would have been impossible for me to carry out my study.

SUMMARY (in Japanese)

木材細胞壁において，セルロースは高度に結晶化して剛直なミクロフィブリル（CMF）をなす．各ラメラにおいてCMFは規則的に配向し，さらにラメラごとにその配向が異なっていることから木材の力学物性にはCMFの内部構造と物性が大きく反映していると考えられる．さらに，木材細胞壁において，CMFはヘミセルロースとリグニンからなるマトリックス物質に包み込まれているから，木材の力学物性の発現はマトリックス物質の構造および物性も少なからず関与しているだろう．

例えば，木材の力学物性には温度および水分が大きく影響する．その作用機序はセルロース，リグニンおよびヘミセルロースといった個々の細胞壁構成要素の分子レベルでの温度・水分物性から還元的に解明されるべきである．

細胞壁構成要素の構造や物性については，単離した木材構成成分を用いた研究のほか，藻類や靱皮繊維のCMFから得られた知見をもとに興味深い考察がなされている．しかしながら，そのほとんどが個別的現象論にとどまっており，巨視的レベルで木材が示す種々の力学物性を矛盾なく説明するには至っていない．その最大の理由は，木材細胞壁の分子レベルでの複合構造の理解に不足があること，特にCMFとマトリックス物質との界面構造が実質的には未解明であるということが挙げられる．このような状況においては，分子レベルからのアプローチによって観察・測定データが得られたとしても，それを細胞壁あるいは木材の挙動にまで演繹するようなモデルは組み立てられない．

なお木材のレオロジー現象のいくつかはしばしば補強マトリックス仮説によってモデル化される．これは，細胞壁ラメラをCMFの強化相とマトリックス物質の母材相とで二相近時し，両者の力学的相互作用を定めるものである．そういった意味から考えると，細胞（壁）以上のオーダーの現象を記述する解析方法であって，CMFやマトリックスの内部構造や物性について言及するものではない．

ところで，補強マトリックス仮説から導かれる木材細胞（壁）モデルには各種パラメータが含まれており，個々の細胞壁構成要素の挙動や物性はこれらの中に分散されて折り込まれている．シミュレーションを行い，結果を観測事実と比較する時に，各種パラメータを合理的に決定しなければならないが，これ

らの値は細胞壁構成要素のミクロな性質をなんらかの形で示しているはずである．すなわち，パラメータの合理性を検討することによって，CMF やマトリックス物質のさまざまな挙動が，いわば逆解析的に浮かび上がってくるのではないかとも期待できる．

以上のことを背景として，本論文では，木材の各種物性と細胞壁微細構造との関連性について研究を行った．各種物性の中でも特に繊維方向の挙動を知ることは大変重要である．なぜなら繊維方向の物理特性は細胞壁構成要素の特徴を直接反映しているためである．本研究においては，繊維方向の弾性的性質および粘弾性的性質に焦点を絞って研究を進めてきた．

第１章では，木材の持つ各種物性（弾性的性質，粘弾性的性質）に関するこれまでの研究についてまとめた．

第２章では，単離した木部繊維の繊維方向ヤング率を記述するためのモデルを構築し，木材の弾性的性質に関するいくつかのケーススタディーを行った．従来，繊維方向ヤング率の含水率依存性は主に細胞壁構成要素の中のマトリックス物質の水分物性によって支配されていると考えられてきたが，提案したモデルを用いてシミュレーションを行ったところ，マトリックス物質のヤング率の値として不合理な値を設定しなければならないことが明らかとなった．これを回避するために，細胞壁構成要素である CMF の構造についてある仮説を提案した．それは，「細胞壁中の CMF が安定な結晶相，安定な非晶相，不安定な相の 3 相からなる」という仮説である．不安定な相のセルロースは乾燥状態では力学的に見て結晶と同じである（擬結晶状態）が，その内部の水素結合は侵入してきた水分子によって容易に断ち切られ，水を含んだ状態では非晶状態とふるまうもの（擬非晶状態）とする．この仮説に基づいてシミュレーションを行った場合，繊維方向ヤング率の含水率依存性は定量的に説明可能となった．その他にも考えられうる仮説を提案したが，次章において否定された．

第３章では，第２章で提案した繊維方向ヤング率の含水率依存性を説明する仮説の整合性を実験的・理論的両観点から検討した．本研究に用いた細胞モデルは一本の木部繊維を模式化したものであるために，よりモデルに近い形状の試験片を用いた実測が必要となる．そこで，スギ早材部位からスライディングミクロトームを用いて均一な薄試験片を採取し，これを繊維細胞モデルに近似しうるものと考えて，繊維方向ヤング率の含水率依存性を実測した．測定され

た繊維方向ヤング率は低含水率領域では非常に高く，水分吸着に伴ってその値は減少していき，繊維飽和点以上の高含水率域で一定となる典型的な含水率依存性を示した．また第2章で提案した仮説の一つである「木材細胞壁中のマトリックス物質のヤング率は単離して測定された値よりも全乾状態で数倍大きくなっている」ということの是非をも検討するために，水分吸着による繊維方向ヤング率の減少率をMFAとの関連で測定した．もし，この仮説が正しいならば，ヤング率の減少率はMFAが小さな試験片よりもMFAが大きい場合においてより顕著になるはずである．しかしながら，ヤング率の減少率はMFAの大きさに関係なくほぼ一定，もしくはMFAが小さい場合の方が顕著であるという結果が得られた．この結果は「木材細胞壁中のマトリックス物質のヤング率は単離して測定された値よりも全乾状態で数倍大きくなっている」という仮説を否定するものであると考えた．また，本研究で測定した繊維方向ヤング率の含水率依存性の実測結果を細胞モデルを用いたシミュレーションにより検討したところ，細胞壁中のCMFに「不安定な相」を仮定することで定量的に実測結果を説明することが可能であり，逆に，不安定な相の存在を仮定せずにシミュレーションを行った場合は実測結果を説明することは不可能となることが明らかとなった．以上の結果から，木材細胞壁を構成しているCMFには安定な結晶と安定な非晶との中間状態としての「不安定な相」が存在しているという結論を得た．

ここまでの研究は木材を弾性体と捉え，繊維方向ヤング率に注目して細胞壁微細構造と関連付けて考察を行ってきた．なお，木材を建築や家具部材として用いる場合に粘弾性挙動を明らかにしておくことは大変重要なことである．しかしながらこれまでの研究において，繊維方向引張における粘弾性挙動の報告はほとんどない．つまり繊維方向引張における粘弾性挙動と細胞壁微細構造との関連性はほとんど未解明のままにおかれている．

そこで，第4章では，スギ早材部位から採取したミクロトーム試験片を用いて繊維方向引張クリープ挙動を実測し，細胞壁微細構造との関連で考察を行った．従来報告されている曲げ試験や横圧縮試験による結果と同様に，繊維方向引張クリープ挙動は負荷と同時に瞬間コンプライアンス（瞬間変形）を生じ，その後，時間経過に伴って変形が増加して，数百時間後には一定となった．また繊維方向引張クリープ挙動のMFA依存性および含水率依存性を検討した結果，両者に対し高い依存性を示すことが明らかとなった．その原因として，繊維方

向引張における物理的挙動は細胞壁構成要素の性質とそれらの空間的配置のあり方を直接的に反映することが挙げられる．つまり，MFA が小さい木部繊維の場合には，繊維方向の物性は主に水分の影響を受けないであろう CMF の挙動を直接に反映し，クリープ変形量は小さくなる．一方，MFA が大きい場合には CMF の影響が小さくなり，水分の影響を受けやすいマトリックス物質の影響が顕著となる．そのためにクリープ変形量は MFA が小さい場合に比べ数倍以上にも大きくなると考えられる．また，粘弾性モデルを用いた解析ではモデルを構成する個々のパラメータが MFA と含水率の両者に強く依存することが分かった．しかしながら，用いた粘弾性モデルではパラメータの値は決定できても，それらと現実の細胞壁構成要素との対応関係は必ずしも明確ではない．今後，現実の木部繊維の構造に近い力学モデルを用いることによって個々の細胞壁構成要素の粘弾性挙動を明らかにしていく必要がある．第 3 章で導入・定式化した多層木部繊維モデルがその契機となるものと期待する．

本研究では，木材の繊維方向の力学物性と細胞壁微細構造との関連性について実験および理論的手法を用いて考察を行い，細胞壁構成要素の性質を明らかにした．本論文で提案した研究手法と，それを用いることによって得られた結果は，木材の持つより多くの性質を統一的に説明できるモデルの構築と，それを用いることで CMF，マトリックス物質の微細構造と物性および両者の界面構造のあり方を解明する研究へと直接につながるものと期待される．

APPENDIX

1: Details of the various coefficients in the equations

$\tilde{e}$, $\tilde{q}$ and $\tilde{r}$ in Eq.2-13" are

$$\tilde{e}=1+\frac{2}{3}G_{\mathrm{u}}-\frac{1}{3}G_{\mathrm{u}}^{2}\left\{\left(\frac{u}{u^{2}-1}\ln u\right)^{2}-\frac{1}{4}\right\},\quad \tilde{q}=\frac{1}{3(u^{2}-1)}\left\{2G_{\mathrm{u}}\frac{u^{2}}{u^{2}-1}(\ln u)-(2+G_{\mathrm{u}})\right\},$$

$$\tilde{r}=\frac{u}{3(u^{2}-1)}\left\{2+G_{\mathrm{u}}-2G_{\mathrm{u}}\frac{1}{u^{2}-1}(\ln u)\right\}$$

e, q and q^* in Eq.2-13"' are

$$e=1+\frac{2}{3}G_{S}(1-3\sin^{2}\theta+3\sin^{4}\theta)-\frac{1}{3}G_{S}^{2}\sin^{4}\theta(2-3\sin^{2}\theta)^{2}\left\{\left(\frac{k}{k^{2}-1}\ln k\right)^{2}-\frac{1}{4}\right\},$$

$$q=\frac{k^{2}}{3(k^{2}-1)}\left\{2+G_{S}\sin^{4}\theta+2G_{S}\sin^{2}\theta(2-3\sin^{2}\theta)\frac{\ln k}{k^{2}-1}\right\},$$

$$q^{*}=-\frac{1}{3(k^{2}-1)}\left\{2+G\sin^{4}\theta+2G\sin^{2}\theta(2-3\sin^{2}\theta)\frac{k^{2}}{k^{2}-1}\ln k\right\}$$

a, b and p in Eq.2-15 are

$$a=1+\frac{2}{3}G_{\mathrm{u}}-\frac{1}{3}G_{\mathrm{u}}^{2}\left\{\left(\frac{u}{u^{2}-1}\ln u\right)^{2}-\frac{1}{4}\right\}+G_{\mathrm{u}}G_{\mathrm{l}}\left(\frac{u^{2}}{u^{2}-1}\right)(2+G_{\mathrm{u}})+\frac{2}{3}G_{\mathrm{u}}^{2}G_{\mathrm{l}}\left(\frac{u^{2}}{u^{2}-1}\right)\ln u,$$

$$b=-\frac{4}{3}G_{\mathrm{u}}^{2}G_{\mathrm{l}}(\ln u)\left(\frac{u^{2}}{u^{2}-1}\right)^{2},\quad p=\frac{1}{3(u^{2}-1)}\left\{2G_{\mathrm{u}}\frac{u^{2}}{u^{2}-1}(\ln u)-2-G_{\mathrm{u}}\right\}$$

B and H in Eqs.2-16, 2-19 and 2-20 are

$$B=G_{\mathrm{u}}\left(2+G_{S}\sin^{4}\theta\left(\frac{u^{2}}{u^{2}-1}\ln u\right)+G_{S}(2+G_{\mathrm{u}})\sin^{2}\theta(2-3\sin^{2}\theta\left(\frac{\ln k}{k^{2}-1}\right),\right.$$

$$H=\frac{S_{\mathrm{u}}}{S_{S}}G_{\mathrm{u}}G_{\mathrm{l}}-\frac{1}{4}(k^{2}-1)\left\{G_{S}\sin^{2}\theta(2-3\sin^{2}\theta\left(1-\frac{2}{k^{2}-1}\ln k\right)-2-2G_{S}\sin^{2}\theta\cos^{2}\theta\right\}$$

2: $\hat{L}_0$ in Eq.2-14, L_0 in Eq.2-16

Eliminating the $\hat{L}_0$ term in Eq.2-14

The first formula of the Eqs.2-11 is rewritten as the problem of the CIL layer, and applied the solution of the differential Eq.2-12. Thereafter, we substitute u_2 into r, and consider h as the second ordered infinitesimal quantity, then, obtain

$$2F\,\hat{\varepsilon}_T\big|_{r=u2} = P_3 - F\,\varepsilon_L \tag{A2-1}$$

By using the Eq.2-13', we eliminate P_3, then, obtain the Eq.2-14'. By substituting the Eq.2-14' into Eq.2-14, we can eliminate the $\hat{L}_0$ term in Eq.2-14.

Eliminating the L_0 term in Eq.2-16

The solution of the differential Eq.2-12 is substituted into the first formula of the Eqs.2-11 as the problem of the S2 layer, and solved for P_2 assuming $r=r_2$.Thereafter, P_2 obtained here is substituted into the Eq.2-13''', then L_0 can be solved as follows.

$$\begin{aligned}
&\frac{2}{3}\frac{1}{S_S}\frac{1}{r_2^2 - r_1^2}\left(2 + G_S m^4\right)L_0 \\
&= \left[e - \frac{1}{4}q\left(k^2 - 1\right)\left\{ G_S m^2 (2 - 3m^2)\left(1 - 2\frac{1}{k^2 - 1}\ln k\right) - 2 - 2G_S l^2 m^2 \right\} \right]\varepsilon_L \\
&+ \frac{1}{2}q(k^2 - 1)(2 + G_S m^4)\varepsilon_T\big|_{r=r2}
\end{aligned} \tag{A2-2}$$

The Eq.2-16 is rewritten eliminating the terms of L_0, and the Eq.2-17 is obtained.

3: Details of the program used by the simulation

(1) The N88-BASIC program calculating the relationship between the MFA and the Longitudinal Young's modulus

Program's title "YANGMFA2.bas"

```
10  ' save "YANGMFA2.bas".
20  CLS 3
30  CONSOLE 0,25,1,0:SCREEN 2 :CLS:PRINT "PLEASE STOP THE ROUTINE, AND
RE-INPUT THE DEFAULT VALUES OF THE PARAMETERS, AND RESTART FROM THE
LINE NUMBER 60"
40  PRINT :PRINT
50  LIST 60-97
60 'PARAMETERS OF THE COMPONENTS AT GREEN CONDITION, *10^3 kgf/cm" FOR
ELASTIC.
70  T=1.015 : K=1.165:SIG=50  :HT2=.025  :ECELL=1340  :EMATR=20
80  'PARAMETERS AT OVEN-DRIED CONDITION.
90  SI0=50
95  'CRYSTAL VOLUME RATIOS AT GREEN CONDITION.
97  A=40  : ADASH=20
100'
110  CLS
120  INPUT "MOISTURE CONTENT OF WOOD (%)  ";MC
130  INPUT " DO YOU MAKE DATA FILES (SEQUENTIAL FILES) (Y/N)  ";QUIT1$
140  IF QUIT1$="Y" OR QUIT1$="y" THEN GOTO 150 ELSE GOTO 170
150  INPUT "  GIVE THE NAME OF THE FILES ";NAM$
160  OPEN NAM$+".YAN" FOR OUTPUT AS #1
170  CLS
180  ECELL=ECELL*1000 : EMATR=EMATR*1000
190  SIG=SIG*1000 : SI0=SI0*1000
200  INPUT "VOLUME RATIO OF THE REVERSIBLE DOMAIN (CRYST-AMORP) IN S2 (%)
";L
210  INPUT "VOLUME RATIO OF THE REVERSIBLE DOMAIN (CRYST-AMORP) IN S1 (%)
```

```
";LDASH
220  INPUT "YOUNG MOD. OF THE MATRIX SUBSTANCE AT DRIED CONDITION (*10^3
kgf/cm2)";GUZAI
230  GUZAI=GUZAI*1000
240  DGUZAI=GUZAI-EMATR
250  MFA=-1
270  HIJU=1.5*(K*K*T*T*(1+.5*HT2)-1)/(1+.5*HT2)/K/K/T/T
280  PRINT "DENSITY OF THE MATERIAL"
290  PRINT "R= ";HIJU
300  PRINT "MFA(deg),EL(kgf/cm2),ELW(kgf/cm2),VLT="
310  LINE (320,200)-(560,200):LINE(320,0)-(320,300):LINE (320,0)-(560,0): LINE
(320,300)-(560,300):LINE (560,0)-(560,300)
320  LINE (320,250)-(328,250)
330   LINE (320,100)-(328,100):LINE (320,0)-(328,0):LINE (320,150)-(328,150)
340   LINE (360,192)-(360,200):LINE (400,192)-(400,200):LINE (440,192)-(440,200)
350   LINE (480,192)-(480,200):LINE (520,192)-(520,200)
360   LINE (560,192)-(560,200):LINE (320,50)-(328,50)
370  '
380  '
390  SI=.5*(SI0-SIG)*COS(3.14159*MC/30)+.5*(SI0+SIG)
400
SS=(1/150)*(100-A-.5*L-.5*L*COS(3.14159*MC/30))*(.5*DGUZAI*COS(3.14159*MC/30)+.5*(
EMATR+GUZAI))
410
ST=(1/150)*(100-ADASH-.5*LDASH-.5*LDASH*COS(3.14159*MC/30))*(.5*DGUZAI*COS(3.
14159*MC/30)+.5*(EMATR+GUZAI))
420  YAN2=(1/100)*(A+.5*L*COS(3.14159*MC/30)+.5*L)*ECELL
430  YAN1=(1/100)*(ADASH+.5*LDASH*COS(3.14159*MC/30)+.5*LDASH)*ECELL
440  GS=YAN2/SS
450  GT=YAN1/ST:   SM=SS/ST
460  GI=SI*HT2/YAN1
```

```
465  ==========ROOP FOR CHANGING THE MFA==========
467  MFA=MFA+1
468  M=MFA*3.14159/180
470  S=SIN(M):M2=2*M:S2=SIN(M2):C=SQR(1-S*S):C2=1-2*S*S
480
EI=T*T-1+(2/3)*GT*(T*T-1)-(1/3)*GT*GT*(T*LOG(T)*T*LOG(T)/(T*T-1)-.25*(T*T-1))+GT*G
I*T*T*(2+GT)+(2/3)*GT*GT*GI*T*T*LOG(T)/(T*T-1)
490  KYU=(K*K/3/(K*K-1))*(2+GS*S*S*S*S+2*GS*S*S*(2-3*S*S)*LOG(K)/(K*K-1))
500
E=1+(2/3)*GS*(1-3*S*S+3*S*S*S*S)-(1/3)*GS*GS*S*S*S*S*(2-3*S*S)*(2-3*S*S)*((K*LOG(
K)/(K*K-1))^2-(1/4))
510  PI=(1/3)*(2*GT*T*T*LOG(T)/(T*T-1)-2-GT)
520
BII=GT*(2+GS*S*S*S*S)*T*T*LOG(T)/(T*T-1)+GS*(2+GT)*S*S*(2-3*S*S)*LOG(K)/(K*K-1)
530  BI=-1*(4/3)*GT*GT*GI*T*T*LOG(T)/(T*T-1)
540  CI=(1+GT)*(T*T-1)-GT*GT*(T*T*LOG(T)*LOG(T)/(T*T-1)-.25*(T*T-1))
550  EF=1-GS*S*S*C2+GS*GS*S*S*S*S*S*S*(2-3*S*S)*((K*LOG(K)/(K*K-1))^2-1/4)
560  ZI=(1/3)*GS*(2-3*S*S)-(2/3)*GS*GS*S*S*S*S*(2-3*S*S)*((K*LOG(K)/(K*K-1))^2-1/4)
570  DI=-1*(1/3)*GT*(T*T-1)+(2/3)*GT*GT*(T*T*LOG(T)*LOG(T)/(T*T-1)-.25*(T*T-1))
580
ECHI=GT*GI-(1/4)*SM*(K*K-1)*(GS*S*S*(2-3*S*S)*(1-2*LOG(K)/(K*K-1))-2-2*GS*C*C*S*
S)
590  AI=-1*(3/4)*(K*K-1)*(2+GS*S*S*S*S*(1-2*LOG(K)/(K*K-1)))
600
A11=EI*KYU-E*SM*PI+(2/3)*SM*BII*(E-(1/4)*(K*K-1)*KYU*(GS*S*S*(2-3*S*S)*(1-2*LOG
(K)/(K*K-1))-2-2*GS*C*C*S*S))/(2+GS*S*S*S*S)
610  A12=(1/3)*SM*KYU*BII*(K*K-1)
620  A13=-1*BI*KYU
630  A21=(T*T-1)+2*T*T*ECHI+.5*GT*(T*T-1-2*T*T*LOG(T))
640  A22=(2+GT)*(T*T-1)+SM*T*T*(K*K-1)*(2+GS*S*S*S*S)
650  A23=4*T*T*GT*GI
```

```
660  A31=T*T-1+2*ECHI+(1/2)*GT*(T*T-1-2*LOG(T))
670  A32=SM*(K*K-1)*(2+GS*S*S*S*S)
680  A33=(2+GT)*(T*T-1)+4*GT*GI
690
DA=A11*A22*A33+A12*A23*A31+A13*A21*A32-A11*A23*A32-A12*A21*A33-A13*A22*A
31
700  D11=A22*A33-A23*A32:D12=-A21*A33+A23*A31:D13=A21*A32-A22*A31
710  D21=-A12*A33+A13*A32:D22=A11*A33-A13*A31:D23=-A11*A32+A12*A31
720  D31=A12*A23-A13*A22:D32=-A11*A23+A13*A21:D33=A11*A22-A12*A21
730  EL=3*DA*ST/D11/KYU/(2+GT)/T/T/1.05
740  ELW=EL*(1.05*K*K*T*T/(1.05*K*K*T*T-1))
750  VLT=-D13/D11
760  EL=EL/1000 : ELW=ELW/1000
770  MMFA=MFA/10
780  IF MMFA-INT(MMFA)<.005 THEN 830 ELSE 850
790  'IF MMFA=20 GOTO   690 ELSE 684
800  'IF MMFA=30 GOTO   690 ELSE 686
810  'IF MMFA=40 GOTO   690 ELSE 688
820  'IF MMFA=50 GOTO   690 ELSE 720
830  PRINT
840  PRINT MFA;EL;ELW;VLT
850  '
860  '
870  IF QUIT1$="Y" OR QUIT1$="y" THEN GOTO 880 ELSE GOTO 890
880  WRITE #1,MFA,EL,ELW,VLT
890  'LPRINT :LPRINT
900  '
910  X=320+MFA*4 :YL=200-EL*1 :YT=200-VLT*100
920  CIRCLE (X,YL),2:CIRCLE (X,YT),1
930  IF MFA>59 THEN GOTO 990
940  GOTO 467
```

```
950  '
960  '
970  '
980  '
990  '
1000  IF QUIT1$="Y" OR QUIT1$="y" THEN CLOSE #1 ELSE GOTO 1010
1010  '
1020  '
1030  '
1040  '
1050  '
1060  END
```

(2) The N88-BASIC program calculating the relationship between the moisture content and the longitudinal Young's modulus

Program's title "YANG98-5.bas"

```
10  save "YANG98-5.bas".A
20  CLS 3
30  CONSOLE 0,25,1,0:SCREEN 2 :CLS:PRINT " PLEASE STOP THE ROUTINE, AND
RE-INPUT THE DEFAULT VALUES OF THE PARAMETERS, AND RESTART FROM THE
LINE NUMBER 60"
40  PRINT :PRINT
50  LIST 60-70
60  'PARAMETERS OF THE COMPONENTS AT GREEN CONDITION, *10^3 kgf/cm" FOR
ELASTIC.
70  T=1.015 : K=1.211:SIG=50   :HT2=.025   :ECELL=1340   :EMATR=20
80  'PARAMETERS AT OVEN-DRIED CONDITION.
90  SI0=50
100  '
110  CLS
120  INPUT "MFA IN THE S2 LAYER (DEG.) ";MFA
130  INPUT " DO YOU MAKE DATA FILES (SEQUENTIAL FILES) (Y/N) ";QUIT1$
140  IF QUIT1$="Y" OR QUIT1$="y" THEN GOTO 150 ELSE GOTO 170
150  INPUT "GIVE THE NAME OF THE FILES ";NAM$
160  OPEN NAM$+".YAN" FOR OUTPUT AS #1
170  CLS
180  ECELL=ECELL*1000 : EMATR=EMATR*1000
190  SIG=SIG*1000 : SI0=SI0*1000
193  INPUT "VOLUME RATIO OF THE CONSTANT CRYSTAL CELLULOSE IN S2 (%)";CR
195  INPUT "VOLUME RATIO OF THE CONSTANT CRYSTAL CELLULOSE IN S1 (%)
";CRDASH
200  INPUT "VOLUME RATIO OF THE REVERSIBLE DOMAIN (CRYST-AMORP) IN S2 (%)
";L
210  INPUT "VOLUME RATIO OF THE REVERSIBLE DOMAIN (CRYST-AMORP) IN S1 (%)
```

```
";LDASH
220  INPUT "YOUNG MOD. OF THE MATRIX SUBSTANCE AT DRIED CONDITION (*10^3
kgf/cm2) ";GUZAI
225  GUZAI=GUZAI*1000
230  DGUZAI=GUZAI-EMATR
240  '
250  M=MFA*3.14159/180
260  HIJU=1.5*(K*K*T*T*(1+.5*HT2)-1)/(1+.5*HT2)/K/K/T/T
270  PRINT "DENSITY OF THE MATERIAL"
280  PRINT "R= ";HIJU
290  PRINT "MC(%), EL(kgf/cm2), ELW(kgf/cm2), VLT="
300  LINE (320,200)-(560,200):LINE (320,0)-(320,300) :LINE (320,0)-(560,0): LINE
(320,300)-(560,300):LINE (560,0)-(560,300)
310  LINE (320,250)-(328,250)
320  LINE (320,100)-(328,100):LINE (320,0)-(328,0):LINE (320,150)-(328,150)
330  LINE (360,192)-(360,200):LINE (400,192)-(400,200):LINE (440,192)-(440,200)
340  LINE (480,192)-(480,200):LINE (520,192)-(520,200)
350  LINE (560,192)-(560,200):LINE (320,50)-(328,50)
360  FOR I=0 TO 150
370  MC=.2*I
380  SI=.5*(SI0-SIG)*COS(3.14159*MC/30)+.5*(SI0+SIG)
390
SS=(1/150)*(100-CR-.5*L-.5*L*COS(3.14159*MC/30))*(.5*DGUZAI*COS(3.14159*MC/30)+.5*
(EMATR+GUZAI))
400
ST=(1/150)*(100-CRDASH-.5*LDASH-.5*LDASH*COS(3.14159*MC/30))*(.5*DGUZAI*COS(3
.14159*MC/30)+.5*(EMATR+GUZAI))
410  YAN2=.01*(.5*L*COS(3.14159*MC/30)+.5*L+CR)*ECELL
420  YAN1=.01*(.5*LDASH*COS(3.14159*MC/30)+.5*LDASH+CRDASH)*ECELL
430  GS=YAN2/SS
440  GT=YAN1/ST: SM=SS/ST
```

```
450  GI=SI*HT2/YAN1
460  S=SIN(M):M2=2*M:S2=SIN(M2):C=SQR(1-S*S):C2=1-2*S*S
470
EI=T*T-1+(2/3)*GT*(T*T-1)-(1/3)*GT*GT*(T*LOG(T)*T*LOG(T)/(T*T-1)-.25*(T*T-1))+GT*G
I*T*T*(2+GT)+(2/3)*GT*GT*GI*T*T*LOG(T)/(T*T-1)
480 KYU=(K*K/3/(K*K-1))*(2+GS*S*S*S*S+2*GS*S*S*(2-3*S*S)*LOG(K)/(K*K-1))
490
E=1+(2/3)*GS*(1-3*S*S+3*S*S*S*S)-(1/3)*GS*GS*S*S*S*S*(2-3*S*S)*(2-3*S*S)*((K*LOG(
K)/(K*K-1))^2-(1/4))
500  PI=(1/3)*(2*GT*T*T*LOG(T)/(T*T-1)-2-GT)
510
BII=GT*(2+GS*S*S*S*S)*T*T*LOG(T)/(T*T-1)+GS*(2+GT)*S*S*(2-3*S*S)*LOG(K)/(K*K-1)
520  BI=-1*(4/3)*GT*GT*GI*T*T*LOG(T)/(T*T-1)
530  CI=(1+GT)*(T*T-1)-GT*GT*(T*T*LOG(T)*LOG(T)/(T*T-1)-.25*(T*T-1))
540  EF=1-GS*S*S*C2+GS*GS*S*S*S*S*S*S*(2-3*S*S)*((K*LOG(K)/(K*K-1))^2-1/4)
550  ZI=(1/3)*GS*(2-3*S*S)-(2/3)*GS*GS*S*S*S*S*(2-3*S*S)*((K*LOG(K)/(K*K-1))^2-1/4)
560  DI=-1*(1/3)*GT*(T*T-1)+(2/3)*GT*GT*(T*T*LOG(T)*LOG(T)/(T*T-1)-.25*(T*T-1))
570
ECHI=GT*GI-(1/4)*SM*(K*K-1)*(GS*S*S*(2-3*S*S)*(1-2*LOG(K)/(K*K-1))-2-2*GS*C*C*S*
S)
580  AI=-1*(3/4)*(K*K-1)*(2+GS*S*S*S*S*(1-2*LOG(K)/(K*K-1)))
590
A11=EI*KYU-E*SM*PI+(2/3)*SM*BII*(E-(1/4)*(K*K-1)*KYU*(GS*S*S*(2-3*S*S)*(1-2*LOG
(K)/(K*K-1))-2-2*GS*C*C*S*S))/(2+GS*S*S*S*S)
600  A12=(1/3)*SM*KYU*BII*(K*K-1)
610  A13=-1*BI*KYU
620  A21=(T*T-1)+2*T*T*ECHI+.5*GT*(T*T-1-2*T*T*LOG(T))
630  A22=(2+GT)*(T*T-1)+SM*T*T*(K*K-1)*(2+GS*S*S*S*S)
640  A23=4*T*T*GT*GI
650  A31=T*T-1+2*ECHI+(1/2)*GT*(T*T-1-2*LOG(T))
660  A32=SM*(K*K-1)*(2+GS*S*S*S*S)
```

```
670  A33=(2+GT)*(T*T-1)+4*GT*GI
680
DA=A11*A22*A33+A12*A23*A31+A13*A21*A32-A11*A23*A32-A12*A21*A33-A13*A22*A
31
690  D11=A22*A33-A23*A32:D12=-A21*A33+A23*A31:D13=A21*A32-A22*A31
700  D21=-A12*A33+A13*A32:D22=A11*A33-A13*A31:D23=-A11*A32+A12*A31
710  D31=A12*A23-A13*A22:D32=-A11*A23+A13*A21:D33=A11*A22-A12*A21
720  EL=3*DA*ST/D11/KYU/(2+GT)/T/T/1.05
730  ELW=EL*(1.05*K*K*T*T/(1.05*K*K*T*T-1))
740  VLT=-D13/D11
750  EL=EL/1000 : ELW=ELW/1000
760  MMC=MC/10
770  IF MMC-INT(MMC)<.01 THEN 820 ELSE 840
780  'IF MFA=20 GOTO   690 ELSE 684
790  'IF MFA=30 GOTO   690 ELSE 686
800  'IF MFA=40 GOTO   690 ELSE 688
810  'IF MFA=50 GOTO   690 ELSE 720
820  PRINT
830  PRINT MC;EL;ELW;VLT;SS,ST,YAN2,YAN1
840  '
850  '
860  IF QUIT1$="Y" OR QUIT1$="y" THEN GOTO 870 ELSE GOTO 880
870  WRITE #1,MC,EL,VLT
880  'LPRINT :LPRINT
890  '
900  X=320+MC*8 :YL=200-EL*1 :YT=200-VLT*100
910  CIRCLE (X,YL),2:CIRCLE (X,YT),1
920  NEXT I
930  '
940  '
950  '
```

```
960  '
970  '
980  '
990  IF QUIT1$="Y" OR QUIT1$="y" THEN CLOSE #1 ELSE GOTO 1000
1000 '
1010 '
1020 '
1030 '
1040 '
1050 END
```

LIST OF PUBLICATIONS CONCERNING THE THESIS

1. *Kojima, Y.*, H.Yamamoto.2002 Properties of the cell wall constituents in relation to the longitudinal elasticity of wood. Part1. Formulation of the longitudinal elasticity of an isolated fiber. Wood Science and Technology. 36: 55-74

2. *Kojima, Y.*, H.Yamamoto. Properties of the cell wall constituents in relation to the longitudinal elasticity of wood. Part2. Origin of the moisture dependency of the longitudinal elasticity of wood. Wood Science and Technology.
(DOI: 10.1007/s00226-003-0177-5, published Online, 2004)

3. *Kojima, Y.*, H.Yamamoto. Effect of microfibril angle on the longitudinal tensile creep behavior of wood. Journal of Wood Science.
(In press, DOI: 10.1007/s10086-003-0565-3)

4. *Kojima, Y.*, H.Yamamoto. Effect of moisture content on the longitudinal tensile creep behavior of wood. Journal of Wood Science. (To be submitted)

LIST OF OTHER PUBLICATION

1. *Kojima,Y.*, H.Yamamoto. T. Okuyama, W. P. Abasolo, J. Gril. 2002 Origin of the biomechanical properties of wood related to the fine structure of the multi-layered cell wall. Journal of Biomechanical Engineering. Transactions of the ASME. 124: 432-440